Clim. Past Discuss., doi:10.5194/cp-2016-24, 2016
Manuscript under review for journal Clim. Past
Published: 17 March 2016


Climate of the Past
Discussions
Open Access
EGU

# An investigation of carbon cycle dynamics since the Last Glacial Maximum: Complex interactions between the terrestrial biosphere, weathering, ocean alkalinity, and $CO_2$ radiative warming in an Earth system model of intermediate complexity

**Simmons, CT[1]; Mysak, LA[2]; Matthews, HD[1]**

1. Department of Geography, Planning and Environment, Concordia University,
1445 Boul. de Maisonneuve Ouest, H1255-26, Montréal, Québec, Canada H3G 1M8

2. Department of Atmospheric and Oceanic Sciences, McGill University,
805 Rue Sherbrooke Ouest, Montréal, Québec, Canada H3A 0B9

Corresponding author: C.T. Simmons, christophesimmons@gmail.com

## Key Words

Earth system modeling, glacial-interglacial change, deglaciation, sensitivity simulations, carbon dioxide, post-glacial terrestrial uptake, ocean alkalinity

Clim. Past Discuss., doi:10.5194/cp-2016-24, 2016
Manuscript under review for journal Clim. Past
Published: 17 March 2016


Climate of the Past Discussions
Open Access
EGU

# Abstract

Proxy reconstructions and modeling studies of the glacial-interglacial changes in the global carbon cycle have led to a stimulating debate in the paleoclimate literature about the mechanisms leading to a 90-100 ppmv increase in atmospheric $CO_2$. In this paper, we used the University of Victoria Earth System Climate Model v. 2.9 to simulate the carbon cycle response to ice sheet retreat and Milankovitch (insolation) forcing from the Last Glacial Maximum (LGM) to the present. In addition, we conducted sensitivity studies to address the contributions of $CO_2$ radiative forcing, atmospheric carbon content, and weathering rates to climate and carbon cycle changes since 21 kyr BP. The simulations show that ice sheet and orbital changes by themselves do not lead to a notable increase in atmospheric $CO_2$ over the course of deglaciation. However, with the application of $CO_2$ radiative forcing and different weathering rates, the simulated atmospheric $CO_2$ variations ranged over ~35 ppmv. Virtually all of the simulated net global vegetation carbon uptake since the LGM is attributable to $CO_2$ fertilization rather than greater land availability or warmer temperatures. Furthermore, the 'greening' from $CO_2$ fertilization significantly enhances total deglacial warming (by 0.14°C) and contributes to warmer intermediate and deep ocean temperatures during the interglacial period. We also found that $CO_2$ radiative forcing was the dominant factor allowing for greater outgassing at the ocean surface and an earlier ventilation of deep-ocean DIC. The downwelling of high-alkalinity surface waters stimulated by a stronger, earlier overturning circulation led to greater deep sedimentation (alkalinity removal), which, in turn, permitted $CO_2$ to continue to increase through much of the simulation period.

Clim. Past Discuss., doi:10.5194/cp-2016-24, 2016
Manuscript under review for journal Clim. Past
Published: 17 March 2016


Climate of the Past Discussions
Open Access
EGU

# 1 Introduction

Significant changes in the carbon cycle following glacial terminations are well-documented in ice core records of atmospheric $CO_2$ (Petit et al.1999; Monnin et al. 2001; Marcott et al. 2014); however, identifying the mechanisms that dominate these changes has proven to be a challenge. Different hypotheses suggest that oceanic, terrestrial, and geological (volcanic) sources of carbon may have contributed to the observed 90-100 ppmv increase in atmospheric $CO_2$ over the course of deglaciation (Simmons et al. 2016, in preparation).

With respect to oceanic sources of carbon, large changes in ocean stratification (Adkins et al 2002; Duplessy et al. 2002; Hodell et al. 2003), vertical mixing (Watson and Naveira Garabato 2006) and water mass distributions (Marson et al. 2014) between the LGM and the present suggest that major circulation changes may have occurred during deglaciation, leading to a large ventilation and outgassing of glacial deep-ocean respired $CO_2$ to the atmosphere (e.g., Galbraith et al. 2007; Jaccard et al. 2009). The greater vertical mixing and upwelling of carbon-rich glacial deep water may have been enhanced dynamically by poleward-shifted (Toggweiler et al. 2006) or stronger (D'Orgeville et al. 2010) Southern Hemisphere westerlies during deglaciation, as well as reduced Southern Ocean seasonal ice cover (Stephens and Keeling 2000; Roche et al. 2012). Furthermore, increasing sea surface temperatures from the LGM to the pre-industrial era would have decreased the solubility of $CO_2$ in sea water, contributing to a net ~10-20 ppmv increase in atmospheric $CO_2$ after accounting for the compensatory effect of ocean freshening (Kohfeld and Ridgwell 2009; Brovkin et al. 2012; Menviel et al. 2012). This gradual surface ocean warming may have also caused a decrease in the remineralization depth of falling

Clim. Past Discuss., doi:10.5194/cp-2016-24, 2016
Manuscript under review for journal Clim. Past
Published: 17 March 2016




organic matter, leading to more respiration nearer to the ocean surface and less trapping of respired $CO_2$ in the deep ocean (Menviel et al. 2012). In addition, less dust/iron transport to and nutrient availability in the surface ocean following a glacial termination (Lambert et al. 2008) may have led to a weaker biological pump during the deglacial period (Parekh et al. 2008; Galbraith and Jaccard 2015). Finally, the flooding of continental shelves would have led to greater shallow-water sedimentation (Brovkin et al. 2012) and coral reef formation (Ridgwell et al. 2003), allowing for long-term ocean alkalinity decreases, which would play its own role in reducing ocean $CO_2$ uptake during the interglacial period.

Other studies have highlighted terrestrial and volcanic contributions to the observed deglacial increase in atmospheric $CO_2$ concentrations. For example, recent estimates of changes in terrestrial carbon stocks (Peterson et al. 2014; Ciais et al. 2012) suggest that the biosphere sequestered a net ~330 Pg C between the LGM and pre-industrial period. At the same time, peatland uptake (400-600 Pg C) since the beginning of the Holocene (~11000 BP) (Yu 2011) and vegetation uptake (~550-694 Pg C in Prentice et al. 2011) were probably much greater. Thus, the relatively modest net uptake of ~330 Pg C since the LGM suggests that a large terrestrial release to the atmosphere occurred during the deglacial period, and likely from a passive soil carbon reservoir, followed by a larger resequestration by the terrestrial biosphere during the interglacial (Ciais et al. 2012). Much of this carbon released during the deglacial period was likely sourced from glacial peatlands and permafrost (which extending to the mid-latitudes during the Last Glacial Maximum) and vegetation growing along now-flooded continental shelves (see Montenegro et al. 2006; Prentice and Harrison 2009; Zech 2012; Köhler et al. 2014; Simmons et al. 2015; Brovkin et al. 2016). In addition, proxy records suggests that enhanced volcanic activity and $CO_2$ emissions (associated with mantle decompression from ice sheet retreat) may

Clim. Past Discuss., doi:10.5194/cp-2016-24, 2016
Manuscript under review for journal Clim. Past
Published: 17 March 2016




have provided a significant source of carbon to the atmosphere during the early Holocene (Huybers and Langmuir 2011), potentially helping maintain elevated atmospheric $CO_2$ concentrations in the wake of accelerated terrestrial uptake from peatland and boreal forest expansion (Roth and Joos 2012; Broecker et al. 2015).

In this paper we analyze the results of a transient run of the UVic ESCM v. 2.9 for the entire period from the LGM to the present, with the purpose of evaluating the carbon cycle response to dominant, well-documented physical and thermodynamic changes in the Earth System over the period: ice sheet extent/height, insolation, and atmospheric $CO_2$-related radiative forcing and carbon content. In particular, we discuss simulations that (1) allow the model's climate and carbon cycles to respond to the changes in the model-calculated $CO_2$, (2) include (solely) the $CO_2$ radiative forcing from ice cores and (3) include a prescribed atmospheric carbon content (which injects enough carbon into the model atmosphere to satisfy the demands of other carbon reservoirs and produce the observed increase in atmospheric $CO_2$ content). The distinction between the three types of modeling experiments helps distinguish processes related to $CO_2$ warming and $CO_2$ carbon content that contribute to climate changes that enhance initial increases in atmospheric $CO_2$.

The results presented here build on past work using the UVic model, which explored relatively short-term glacial (e.g., Schmittner et al. 2007; Schmittner and Galbraith, 2008) and deglacial changes (Huiskamp and Meissner 2012; D'Orgeville et al. 2010). Because we have performed a transient simulation for the entire deglacial period using a model with sediments (Eby et al. 2009), we have been able to investigate the alkalinity feedbacks on the deglacial $CO_2$ rise. In particular, we carried out sensitivity experiments to explore deglacial and interglacial changes with two different (constant) weathering rates. These simulations were compared with

Clim. Past Discuss., doi:10.5194/cp-2016-24, 2016
Manuscript under review for journal Clim. Past
Published: 17 March 2016




other modeling experiments where alkalinity was held constant (weathering set equal to sedimentation), thus isolating the collective contribution of alkalinity to $CO_2$ changes.

Below we provide a brief description of the model (Section 2.1) and the details of our equilibrium simulation for the LGM (Section 2.2). The experimental design for transient simulations of the period is given in Sections 2.3-2.5. Then, in Section 3, we discuss the results for a suite of simulations, including a comparative analysis of the relative contribution of weathering rate, $CO_2$ radiative forcing, and $CO_2$ carbon content to the global carbon cycle. The major conclusions are given in Section 4.

# 2 Model and Methodology

## 2.1 Model Description

The University of Victoria Earth System Climate Model (UVic ESCM, or simply UVic model) v. 2.9 provides a simplified but detailed representation of the Earth's climate system and carbon cycle and is classified as an Earth system Model of Intermediate Complexity (EMIC) (Claussen et al. 2002). All components of the model operate on a grid of 1.8° latitude by 3.6° longitude. The core of the model is a three-dimensional primitive equation ocean general circulation model (the Modular Ocean Model v. 2.0, see Pacanowski (1995)) with 19 vertical levels, coupled to a dynamic-thermodynamic sea ice module (Weaver et al. 2001). Eddy transport is parameterized according to Gent and McWilliams (1990), and diapycnal ocean (vertical) mixing is accomplished through a time-independent horizontally-constant diffusivity profile (approximately 0.3 $10^{-4}$ $m^2$ $s^{-1}$ at the pycnocline). In its present configuration, the model's ocean regime is defined by unchanging present-day bathymetry and sea level, and thus some important features of LGM and deglacial topography, such as continental shelves above

Clim. Past Discuss., doi:10.5194/cp-2016-24, 2016
Manuscript under review for journal Clim. Past
Published: 17 March 2016




sea level, are not featured in the simulations discussed here. However, a closed Bering Strait is a feature of these simulations

Concerning ocean chemical properties, inorganic carbon chemistry and air-sea exchanges of $CO_2$ (controlled by temperature, salinity, DIC, alkalinity, wind speed, and sea ice cover) are described in Ewen et al. (2004). Contributions of the biological pump to the ocean carbon cycle are calculated by a Nutrient-Phytoplankton-Zooplankton-Detritus (NPZD) module, which includes both nitrates and phosphates as well as nutrient recycling through microbial respiration and differential treatment of dissolved and particulate organic carbon (POC) (Schartau and Oschlies 2003; Schmittner et al. 2005; Schmittner et al. 2008). An important update to the 2.9 version of the UVic ESCM is the inclusion of an oxic-only sediment module from Archer (1996), which allows the model to evaluate secondary changes in ocean chemistry and atmospheric $CO_2$ due to sediment respiration and calcium carbonate compensation, although without the effect of coral reefs (Eby et al. 2009). In this model, the dissolution of $CaCO_3$ in falling detritus occurs with an e-folding depth of 3500 m (Schmittner et al. 2008). Once reaching the ocean floor, total $CaCO_3$ dissolution depends on the respired $CO_2$ content of overlying waters and the $CaCO_3$:POC rain ratio at the sediment level (which is calculated as the amount of unrespired organic carbon to calcite content of falling detritus that reaches the ocean floor). Changes in the rain ratio are constrained in the model to lie between 0.55 and 1.82 due to the buffering capacity of sediments (Ridgwell 2003) and the neglect of $CaCO_3$ ballasting effects in the current version of the model. In our simulations, however, the rain ratio does not actually vary significantly (1.05-1.27). It should be noted that all sedimentation occurs at or below a depth of 1240 m, and thus variations in shallow water sedimentation (with increasing sea level) are not parameterized in these simulations.

Clim. Past Discuss., doi:10.5194/cp-2016-24, 2016
Manuscript under review for journal Clim. Past
Published: 17 March 2016




The model atmosphere is simplified to a two-dimensional Energy-Moisture Balance Model (EMBM) (Fanning and Weaver 1996; Weaver et al. 2001). Surface wind fields must be prescribed in order to drive horizontal moisture advection and the wind stress over the ocean. All simulations in this paper use a dampened version of the "wind feedback" in Weaver et al. (2001), which provides a thermal-wind adjustment to 20$^{th}$century reanalysis winds (Kalnay et al. 1996) based on the model-generated spatial temperature gradient at each time step. The atmospheric $\Delta^{14}C$ was kept constant at 0‰ for all simulations, and thus the oceanic $\Delta^{14}C$ profiles generated by the model are mostly a function of ocean ventilation changes. The fractionation ratio $\delta^{13}C$ is not traced in the current version of the model for either the atmosphere or the ocean.

Vegetation changes on land are driven by the Top-down Representation of Interactive Foliage and Flora Including Dynamics (TRIFFID) Module, which represents five plant functional types (PFTs) : $C_3$-photosynthesis grasses (manifested as mid-latitude prairie/steppe and very high latitude tundra in the model), $C_4$-photosynthesis grasses (mostly tropical and subtropical savannah in the model), broadleaf trees (tropical and subtropical forest), needleleaf trees (predominately boreal and high-elevation forest), and shrubs (tropical/Mediterranean bushy vegetation and tundra-boreal forest transition regions) (Cox 2001; Meissner et al. 2003; Matthews et al. 2004). The distribution of PFTs is determined by temperature and soil moisture criteria, and in regions where several types of vegetation can grow, Lotka-Volterra equations (predator-prey interspecies competition based ultimately on a tree-shrub-grass dominance hierarchy and net primary production) determine the predominant species for each grid cell. The soil model (MOSES) stores and respires terrestrial carbon litter in a single layer with 1 m depth (Cox et al. 1999). There is no representation of peatlands in the current version of the model.

Clim. Past Discuss., doi:10.5194/cp-2016-24, 2016
Manuscript under review for journal Clim. Past
Published: 17 March 2016




The UVic model also incorporates prescribed continental ice sheets and non-conducting marine ice shelves (represented as a "lid" over the ocean). Their thickness and areal coverage at the LGM and over the course of deglaciation are determined by the ICE-4G dataset (Peltier 2002). The geographical coverage and retreat of these ice sheets is prescribed every 1000 years according to the above data, with no ice melting (except of accumulated snow on or near the ice sheets) as a result of insolation or temperature changes generated by the model. As a result, ice sheet and ice shelf retreat does not produce a freshwater flux into the ocean or onto nearby land surfaces.

## 2.2 LGM Equilibrium Simulation

Slowly-varying atmospheric $CO_2$ and land ice cover make the LGM perhaps the most appropriate time period to generate a model equilibrium climate with constant forcing parameters. We selected a model spin-up start date of 21000 B.C. (~22950 BP), approximately 2000 years before the standard date for the LGM in order to ensure that glacial conditions were adequately captured by the model in transient simulations. Initiated from pre-industrial conditions (the default restart file for the UVic ESCM v. 2.9), this equilibrium simulation was run for 9700 model years with fixed $CO_2$ (191.1 ppm), orbital forcing (the Milankovitch forcing for 22950 BP), and land ice sheets (which are unchanged in the database from LGM-extent ice sheets at 21000 BP) and with the model's wind feedback adjustment to NCEP reanalysis winds. The carbon content of the oceanic, terrestrial, and sediment reservoirs were equilibrated to maintain the constant atmospheric $CO_2$. As these studies focus only on $CO_2$, no adjustments to the $CO_2$ radiative forcing were made to account for lower concentrations of other greenhouse gases (namely $CH_4$ and $N_2O$). In order to maintain the assumption of an equilibrium carbon cycle just prior to the LGM, the weathering flux was set equal to the sedimentation rate in the spin-up

Clim. Past Discuss., doi:10.5194/cp-2016-24, 2016
Manuscript under review for journal Clim. Past
Published: 17 March 2016




simulation (i.e., constant ocean alkalinity and no nascent carbonate compensation at the beginning of transient simulations).

## 2.3 Transient Forcing

` This equilibrium simulation for 22950 BP was then used as the initial conditions for a series of transient simulations exploring deglaciation with time-evolving orbital (Milankovitch) forcing and retreating ice sheets (ICE-4G) from 23000 BP to the present (ice data was interpolated between data points every 1000 years). A complete list of these experiments is provided in Table 1. Incorporating changes in land ice and insolation, Free Carbon (FC) transient simulations allowed the model's carbon reservoirs to evolve freely without any other prescribed forcing beyond evolving ice sheets and insolation changes. The only $CO_2$ radiative forcing in these FC experiments was provided by model-generated atmospheric $CO_2$ concentration and not the observed record from ice cores. Prescribed Carbon (PC) simulations, however, forced the model's carbon reservoirs to equilibriate to the observed ice core record of atmospheric carbon content, following the Vostok record (Petit et al. 1999) from 23000 BP to 7950 BP, Taylor Dome (Indermühle et al. 1999) from 7950 BP to 944 BP and from Law Dome (Etheridge et al. 1996) after 944 BP (as in Simmons et al. 2013). In contrast to the FC experiments, carbon was injected into (or removed from) the atmosphere in the PC simulations to balance the net sources and sinks from other carbon reservoirs (oceans, biosphere, sediments) in order to maintain the interpolated ice core $CO_2$ concentration for that date. A third series of simulations, testing model sensitivity to deglacial $CO_2$ radiative forcing and denoted "CO2rad" in the results discussion, allowed the model carbon cycle to evolve freely but applied the radiative forcing (warming effect) of $CO_2$ according to the ice core record. The $CO_2$ radiative forcing increased from 0 Watts $m^{-2}$ at 20954

Clim. Past Discuss., doi:10.5194/cp-2016-24, 2016
Manuscript under review for journal Clim. Past
Published: 17 March 2016


Climate of the Past Discussions

BP and was calculated from the same ice core record (Vostok and Taylor/Law Domes) as in the PC simulations using the traditional formula ($\Delta F = 5.35 \times \ln(C/C_o)$, where C represents the linearly-interpolated $CO_2$ between data points from the ice core record and $C_o$ represents the $CO_2$ value from Petit et al. (1999) at ~20954 BP).

| Simulation Name | Milankovitch forcing | ICE-4G prescribed land ice | Ice core $CO_2$ radiative forcing starting at 19004 B.C. | Prescribed atmospheric $CO_2$ from ice cores | Weathering Rate = |
|---|---|---|---|---|---|
| ***Transient Simulations described in Section 3.1*** | | | | | |
| FC CA | X | X | | | sedimentation rate |
| FC HW | X | X | | | 144.0 Tg C/yr or 12.0 Tmol/yr |
| FC LW | X | X | | | 120.7 Tg C/yr or 10.1 Tmol/yr |
| CO2rad CA | X | X | X | | sedimentation rate |
| CO2rad HW | X | X | X | | 144.0 Tg C/yr or 12.0 Tmol/yr |
| CO2rad LW | X | X | X | | 120.7 Tg C/yr or 10.1 Tmol/yr |
| | | | | | |
| PC CA | X | X | | X | sedimentation rate |
| PC HW | X | X | | X | 144.0 Tg C/yr or 12.0 Tmol/yr |

*Table 1: A summary of the principal transient simulations discussed in this paper. The acronyms FC CA (free carbon, constant alkalinity), FC HW (free carbon, higher weathering rate), FC LW (free carbon, lower weathering rate), CO2rad CA (CO2 radiative forcing, constant alkalinity), CO2rad HW (CO2 radiative forcing, higher weathering rate), CO2rad LW (CO2 radiative forcing, lower weathering rate), PC CA (prescribed (atmospheric) carbon, constant alkalinity), and PC HW (prescribed (atmospheric) carbon, higher weathering rate) are described in Sections 2.3 and 2.4*

## 2.4 Weathering Rates

Changes in weathering rates can have important implications for ocean alkalinity. However, modeling studies investigating the influence of weathering changes are limited (Brovkin et al. 2012). A comprehensive weathering module is not available in the 2.9 version of the model, but the effects of weathering can be tested indirectly by using different constant weathering rates or by setting the weathering rate equal to the ocean sedimentation rate (the latter of which is determined by the model's coupled ocean biogeochemistry). In simulations where weathering is set equal to sedimentation, denoted henceforth as CA for "constant alkalinity,"

Clim. Past Discuss., doi:10.5194/cp-2016-24, 2016
Manuscript under review for journal Clim. Past
Published: 17 March 2016




there can be no carbonate compensation because weathering inputs directly balance precipitation to the sediments. Simulations with constant alkalinity allow for purely physical mechanisms (and their climate responses) to be isolated from those related to chemical changes in the ocean (alkalinity changes and carbonate compensation). The UVic ESCM, however, does not remove carbon from the terrestrial carbon reservoir (soil erosion) in order to maintain this weathering flux but rather generates new bicarbonate to inject into the ocean. Thus, as the model is currently configured, total carbon conservation is not possible for the constant weathering simulations.

Outside of the CA experiments, one set of simulations uses a "higher" weathering rate (HW) of 12.0 Tmol (Alk)$yr^{-1}$ (or 4566 kg C $s^{-1}$ ), which is the equilibrium weathering rate obtained at the end of the spin-up simulation (Section 2.2). However, in the first 2000 years of both the FC and PC transient simulations (leading up to the actual LGM at 21000 BP), the sedimentation rate dropped abruptly before stabilizing to a lower rate at 21000 BP of ~10.1 Tmol $yr^{-1}$ . Thus, for a second series of "low weathering (LW)" experiments, we used 10.1 Tmol $yr^{-1}$ as a constant weathering rate for the simulation from 21000 BP onward. The range of weathering rates used here may be relatively modest compared to fluctuations in weathering since the LGM.

# 3 Results and Discussion

## 3.1 Atmospheric $CO_2$

The range of processes considered here resulted in $CO_2$ differences of up to 35 ppmv, though none of the simulations reproduced the full magnitude of the observed $CO_2$ increase. The largest increase in $CO_2$ (~25 ppm) from the LGM to the late Holocene is comparable to that obtained by an AOGCM study with a free carbon cycle (Chikamoto et al. 2012). Fig. 1 illustrates the results for transient experiments with the freely-evolving model carbon cycle (FC). Atmospheric $CO_2$ (Fig. 1a) does not increase in any of the simulations without prescribed

Clim. Past Discuss., doi:10.5194/cp-2016-24, 2016
Manuscript under review for journal Clim. Past
Published: 17 March 2016




radiative forcing, indicating that the large changes in land ice (the ice-albedo feedback) and northern hemisphere insolation do not by themselves trigger mechanisms in the model to increase $CO_2$. In fact, for the simulation with constant alkalinity (FC CA) and the higher weathering rate (HW), atmospheric $CO_2$ declines 5-10 ppm from 21000 BP to present.

The results also suggest that the terrestrial carbon reservoir plays an intimate role in the evolution of atmospheric $CO_2$ over the course of these simulations. The decrease in atmospheric $CO_2$ over the period in the FC CA simulation is compensated by a 200 Pg C net increase in the terrestrial carbon since the LGM (Fig 1b, blue line), a figure less than the ~330 Pg C increase estimated by Ciais et al. (2012) and (Peterson et al. 2014). In the same simulation, a compensating transfer of ocean carbon (~195 Pg C) to the atmosphere (Fig. 1b, blue line) is partially hindered by an increase in export production (not shown). The lower constant weathering rate (LW), however, produced a slightly greater atmospheric $CO_2$ (195 ppm) by the mid-Holocene (Fig. 1a, green line). The simulation with the higher constant weathering rate (HW) yielded, in turn, the lowest atmospheric $CO_2$ value just above 180 ppm at the end of the Holocene (Fig. 1a, purple line). The greater weathering is an alkalinity source to the oceans and causes atmospheric $CO_2$ to decrease unless sedimentation (the alkalinity sink) outpaces weathering, whereas lower weathering leads to a decrease in ocean alkalinity if sedimentation outpaces the combined effect of weathering and sediment dissolution (alkalinity sources).

The dip in $CO_2$ in most experiments after 6000 BP (Fig. 1a) occurred in response to a large reduction in Antarctic marine ice shelves. Simmons et al. (2013) showed that, with the disappearance of Antarctic marine ice shelves over the course of an interglacial, open ocean increasingly expanded into the (prescribed) katabatic wind environment around Antarctica, leading to more air-sea exchange, sea ice formation, and brine rejection. This resulted in an

Clim. Past Discuss., doi:10.5194/cp-2016-24, 2016
Manuscript under review for journal Clim. Past
Published: 17 March 2016




enhancement of bottom water formation near the coast of Antarctica, which in turn led to a greater prominence of deep, high-DIC Antarctic bottom waters globally. These denser abyssal waters also led to poorer abyssal ventilation, resulting in an accumulation of DIC at depth and a corresponding drawdown in atmospheric $CO_2$ of about 5 ppm. In a sensitivity study (not shown) of the FC LW simulation with a slightly more extensive ice shelf distribution (as in Simmons et al. 2013), the atmospheric $CO_2$ concentration rose to 199 ppmv between 6000 BP and present rather than the declining further as shown here.

For the simulations including $CO_2$ radiative forcing, a total post-glacial $CO_2$ rise of approximately 15 ppm occurred in the CO2rad CA simulation (Fig. 1a, red line). Compared to the same constant alkalinity simulation without radiative forcing (Fig. 1a, blue line), the net effect of this prescribed warming is 20 ppm more $CO_2$ in the atmosphere. This 20 ppm difference represents the combined effect of both outgassing (from warmer ocean surface temperatures) and deep-ocean ventilation of deep DIC in the model's atmospheric $CO_2$ balance (Fig. 1b, red line). Furthermore, by allowing alkalinity to respond to ocean ventilation changes, the influence of $CO_2$ radiative forcing on the HW and LW profiles led to an even greater increase in $CO_2$ (to 215-230 ppm) due to a notable decrease in both DIC and alkalinity associated with a better-ventilated ocean (Fig. 1a, orange and brown lines).

## 3.2 Terrestrial Carbon

While atmospheric $CO_2$ did not increase markedly in the simulations described above, a more detailed analysis of the changes in vegetation and terrestrial carbon yields some surprising finds. Terrestrial carbon (Fig. 1c) increased just over 200 Pg C in all FC simulations, although Fig. 1d demonstrates that vegetation carbon (above-ground biomass) actually decreased in many

Clim. Past Discuss., doi:10.5194/cp-2016-24, 2016
Manuscript under review for journal Clim. Past
Published: 17 March 2016




runs from the LGM to the early Holocene (11000 BP). The net terrestrial increase after 15000 BP was largely driven by a global increase in soil carbon as ice sheets retreated (Fig. 2c,d). The simulations with $CO_2$ radiative forcing (Fig. 1d, red and orange lines) produced a strong decline in vegetation carbon from the LGM through the early Holocene, in spite of vegetation expansion over formerly ice-covered areas in all of these simulations.

The changes in the spatial distribution of vegetation carbon stocks (Fig. 2a,b) provides additional insight into terrestrial carbon changes. From Figs. 2a,b, we note that terrestrial vegetation gains in mid and high-latitude regions were unable to outweigh larger losses in the tropics (until, at least, the end of the simulation in this FC LW case). The disappearance of ice sheets and related warming slowly destabilized some tropical and subtropical ecosystems. This is particularly true where subtropical boreal forests were replaced by grasslands (such as the present-day southeastern United States, Fig. 2a), resulting in new PFT distributions that accumulated biomass more slowly due to the low atmospheric $CO_2$ in these simulations. Even by the end of the HW simulation (Fig. 2b,d), the model only yielded substantial vegetation and soil carbon gains in areas covered by ice sheets during the LGM; other parts of the world demonstrated equivalent or slightly reduced carbon storage. It should be noted that the UVic's wind feedback is unable to generate a significantly-enhanced African monsoon vegetation (Fig. 2a); thus, the model likely overemphasized the vegetation loss in the Sahel region in the early Holocene. However, the net effect on vegetation carbon should be similar, as most of the African vegetation gains in the mid Holocene were likely lost by the late Holocene (Indermülhe et al. 1999). Other modeling results also suggest that African forests were replaced more readily by low-density forests and shrublands (Fig. 2a) under low glacial $CO_2$ conditions (Jolly and Haxeltine 1997; Street-Perrott et al. 1997). The sensitivity of subtropical and tropical vegetation

Clim. Past Discuss., doi:10.5194/cp-2016-24, 2016
Manuscript under review for journal Clim. Past
Published: 17 March 2016




to less $CO_2$ fertilization thus appears to have had a significant impact on vegetation and terrestrial carbon losses in these simulations, implying that the greater $CO_2$ fertilization over the course of deglaciation was instrumental in maintaining high biomass density in the tropics.

The addition of $CO_2$ radiative forcing to the constant alkalinity experiment led to less vegetation carbon storage than some of the other FC simulations (Fig. 1d), indicating that the global temperature rise associated with both retreating ice sheets and increasing $CO_2$ did not lead to more vegetation carbon storage. The PC simulation (Fig. 3) provides an important comparison, as it injected carbon into the model's carbon reservoirs to force the increase in $CO_2$, but with radiative forcing equivalent to the CO2rad experiment. The physical presence of more carbon in the atmosphere caused substantial net increases in vegetation carbon stocks (by ~230 Pg C, see Fig. 3b), without the decrease in vegetation carbon produced between the LGM and the early Holocene in the FC simulations (Fig. 1d). The total increase in terrestrial carbon of ~600 Pg C in the PC simulations (Fig. 3a) from the LGM to the late Holocene is also comparable in magnitude to that seen in other modeling studies (for example, 550-694 Pg C in Prentice et al. (2011)). The effect of $CO_2$ fertilization turned net terrestrial carbon losses in the tropics in the FC experiments (Fig 2c,d) into carbon gains (Fig 3e,f) and also enhanced carbon storage in subpolar regions.

A secondary effect of the denser and more expansive vegetation resulting from the $CO_2$ fertilization effect led to greater absorption of incoming solar radiation, as seen in comparing the divergence in surface air temperature between the CO2rad HW and the PC HW simulations in Supplementary Fig. 1g (both of which have equivalent $CO_2$ radiative forcing). The biogeophysical impact of greater $CO_2$ fertilization in the PC HW simulation increased SAT globally by ~0.14°C (Supplementary Fig. 1g) and contributed to centennial-scale ocean

Clim. Past Discuss., doi:10.5194/cp-2016-24, 2016
Manuscript under review for journal Clim. Past
Published: 17 March 2016




ventilations that lead to a higher depth-integrated ocean potential temperature (0.12°C) (Supplementary Fig. 1h). The denser tropical vegetation, particularly in South America, Africa, and Southeast Asia (as shown in Fig. 3d), appears to drive much of the fertilization-related increase in global temperature (up to 0.3°C locally, Fig. 4a), as these regions experience a substantial loss in vegetation density without $CO_2$ fertilization. Fig. 4b shows that the temperature difference between the PC CA and CO2rad CA has significant variability in the high latitudes (related to different centennial-scale fluctuations in sea ice and the meridional overturning circulation (MOC)) and an overall zonal-average tropical warming of 0.07-0.2°C. Furthermore, because the tropics are important oceanic upwelling/outgassing regions, the additional warming of the tropics due to the fertilization effect may have a disproportionate influence on the outgassing of $CO_2$. The model's wind feedback also suggests that this warm anomaly driven by $CO_2$ fertilization increases zonal wind speeds in the subtropics (not shown), which adds to the wind stress and dynamical upwelling off the west coasts of South America and Africa (not shown). A deglacial strengthening of the Hadley Cell after the LGM is also suggested by the proxy record (Thompson et al. 1998) and could contribute to poleward shifts in the mid-latitude westerlies (Lamy et al. 2001; Toggweiler et al. 2006).

In summary, the FC simulations (including $CO_2$ radiative forcing) suggest that, without the full $CO_2$ fertilization associated with the observed ice core $CO_2$ trend, modeled vegetation carbon stocks would have been lower following deglaciation than they were during the LGM (contrary to proxy evidence). Total terrestrial carbon did increase (200-250 Pg C) in all free carbon simulations starting at the Pleistocene-Holocene transition, but this feature was largely driven by greater soil carbon storage at high latitudes. The only simulations that support a substantial increase in the photosynthetically-active carbon pool on the scale suggested in Ciais

Clim. Past Discuss., doi:10.5194/cp-2016-24, 2016
Manuscript under review for journal Clim. Past
Published: 17 March 2016




et al. (2012) are the prescribed carbon dioxide (PC) simulations (Fig. 3a). Thus, the results presented here strongly suggest that the carbon sequestration in response to the deglacial rise in $CO_2$ is the most important factor in increasing vegetation biomass between the LGM and present, with vegetation carbon gains at the end of deglaciation and into the Holocene driven by greater $CO_2$ fertilization instead of ice sheet or temperature changes; without a major increase in atmospheric carbon content, vegetation actually decreased during deglaciation and the early Holocene in the UVic model.

## 3.3 Physical and Dynamical Ocean Changes

Over the course of the simulations presented here, the oceans gradually become a net source of atmospheric $CO_2$. The most significant oceanic release of carbon to the atmosphere resulted from the greater warming in the CO2rad simulations. For example, the CO2rad CA scenario yielded 20 ppm more atmospheric $CO_2$ than the FC CA simulation by the mid-Holocene. A comparison of these two simulations reveals that there was ~50 Pg C less terrestrial carbon during deglaciation in the simulation with $CO_2$ radiative forcing (Fig. 1c, red line vs. blue line), and only a small fraction of this was absorbed by the oceans (Fig. 1b). The decreasing ability for the oceans to take up atmospheric $CO_2$ (greater outgassing than uptake) was modulated by warming ocean temperatures (Fig. 5b) by over 2˚C in the CO2rad CA simulation versus only 0.5˚C in the FC CA simulation. This warming was most pronounced at depth, as surface waters vary slightly less over the course of these simulations (1.5-1.6˚C for the CO2rad CA and 0.4-0.5˚C for the FC CA simulation) (Supplementary Figure 2). Solubility considerations (~9 ppm per 1°C warming) mandate that the net effect should be ~9-11 ppm of the ~20 ppm difference in atmospheric $CO_2$ between the FC and CO2rad simulations. These ocean properties do not incorporate the ice melting/ocean freshening effect favouring greater

Clim. Past Discuss., doi:10.5194/cp-2016-24, 2016
Manuscript under review for journal Clim. Past
Published: 17 March 2016




$CO_2$ uptake during deglaciation, as global salinity only decreased by 0.002 ppt as a result of precipitation changes in these experiments.

Complementing the $CO_2$ solubility effect, changes in ocean ventilation also contribute to the higher $CO_2$ levels in the CO2rad simulations. Fig. 5c shows the global maximum overturning streamfunction, which is a general indicator of the strength of North Atlantic Overturning circulation and NADW formation. The PC (Supplementary Fig. 1e) and CO2rad simulations equivalently produced a two-stage increase in the meridional overturning circulation (MOC) strength from LGM values (~15 Sv) to modern values (~21 Sv) by 15500 BP While these simulations lack of freshwater fluxes from retreating ice sheets, the strengthening NADW reflects similar timing as the North Atlantic MOC rebound at the end of Heinrich Event 1 (HE1) around 14500 BP as demonstrated by Pa/Th proxy data (McManus et al. 2004). These modeling results suggest that higher $CO_2$ radiative forcing may have helped accelerate the North Atlantic MOC rebound after HE1. The unforced FC experiments also produced a somewhat stronger (17-18 Sv) meridional overturning circulation around the same time period, but most of these simulations lagged significantly behind the CO2rad MOC recovery, and none of them achieved present-day overturning values. However, all the CO2rad simulations followed the MOC profile from the PC simulation (Supplementary Fig. 1e), indicating that the strength of the MOC rebound to the model's typical modern values was mostly a product of the temperature increase due to the radiative forcing effect of $CO_2$.

The divergence in the $\Delta^{14}C$ trend lines between the FC and CO2rad simulations (Fig. 5b), which lagged the divergence in air temperature between the FC and CO2rad simulations by approximately 1000 years, provides further evidence of a link between $CO_2$ and ventilation changes. The initial increase in $CO_2$ (Fig. 1a) stimulated greater ventilation of deep water from

Clim. Past Discuss., doi:10.5194/cp-2016-24, 2016
Manuscript under review for journal Clim. Past
Published: 17 March 2016




the glacial period, and the ventilation (and warming) of $CO_2$-rich deep waters subsequently led to less oceanic absorption of atmospheric $CO_2$ and eventually a net release (achieved by 9000 BP according to Fig. 1b) from the ocean to the atmosphere from this effect. Fig. 6 illustrates the deep-ocean DIC change for the CO2rad HW simulation at 14500 BP, the approximate timing of post-HE1 recovery and ventilation of the North Pacific (Galbraith et al. 2007), and at 9000 BP, by which time the NADW transport essentially reached its peak and plateaued (McManus et al. 2004). The simulations correspondingly demonstrate a gradual decrease in the DIC content of the Atlantic Ocean relative to the LGM state, with the NADW becoming more prominent and promoting the decrease of DIC in the Indian and South Pacific with time (compare Fig. 6a to Fig. 6b). Related to this ventilation change, proxy evidence of low $\Delta^{14}C$ excursions during the Mystery Interval (~17500 BP to ~14500 BP) indicate an important ventilation (or series of flushes) of the glacial deep ocean during the late Pleistocene. What is new here is that $CO_2$ warming appears to enhance this ventilation.

The model results thus reveal a potential positive feedback relevant to the deglacial rise in $CO_2$, in which an initial increase in temperature due to rising $CO_2$ stimulated a greater ventilation of carbon-rich deep waters, which helped produce an even larger increase in $CO_2$. One potential fast-response mechanism in this feedback loop is sea ice, which is strongly sensitive to warming temperatures and influences overturning. As air-sea gas exchanges are not possible through sea ice in the UVic model, much greater annual sea ice extent in both the northern and southern hemispheres (Fig. 5e-f) could limit convection in both regions (Fig 7). Even without freshwater fluxes, sea ice extent in the North Atlantic was more expansive in the FC simulations after the LGM compared to the CO2rad simulations (Fig 5e), which limited the strength of North Atlantic overturning and deep-water convection in upwelling regions. The FC

Clim. Past Discuss., doi:10.5194/cp-2016-24, 2016
Manuscript under review for journal Clim. Past
Published: 17 March 2016




CA simulation in particular demonstrated less outgassing in tropical upwelling regions at 9000 BP (Fig. 7e), whereas the CO2rad CA simulation showed greater upwelling in the tropics (Fig. 7b,e). Similarly, more sea ice in the Southern Ocean in the FC simulations limited the air-sea exchange of upwelling water masses near Antarctica (Fig. 7e-f).

Fig. 7 also shows that downwelling regions in the North Atlantic (Fig. 7a-b) shifted northeastward over the course of deglaciation in concert with reduced sea ice extent (Fig. 7c-d), whereas upwelling regions (carbon sources to the atmosphere) intensified in the Southern Ocean along retreating sea ice margins, particularly in the CO2rad experiments. Proxy evidence also suggests that this region was likely critical during the upwelling of glacial deep water (Anderson et al. 2009). During the late Holocene, abrupt increase in SH sea ice after 6000 BP in most simulations (Fig. 7f) is a response to a rapid decrease in Antarctic marine ice shelves in the database (described further in Simmons et al. (2013)). This transition was followed by a reduction in atmospheric $CO_2$ associated with a weaker NADW, slowly-ventilating AABW and reduced upwelling (more sea ice) in the Southern Ocean.

In summary, these model results indicate that warming temperatures due to increasing $CO_2$ may have contributed to a decrease in annual-mean sea ice in both hemispheres, which coincided with a faster overturning of model deep waters through the Southern Ocean and stimulated a further rise in $CO_2$. These findings suggest that the Southern Ocean sea ice mechanism described in Stephens and Keeling (2000) may have had some influence in enhancing an ongoing release of carbon from the deep ocean to the atmosphere, especially considering that winter sea ice extent at the LGM was likely much greater than at present (Gersonde et al. 2005; Roche et al. 2012). After accounting for reduced gas solubility with warming SSTs, the sensitivity of atmospheric $CO_2$ to Southern Ocean sea ice area seems similar

Clim. Past Discuss., doi:10.5194/cp-2016-24, 2016
Manuscript under review for journal Clim. Past
Published: 17 March 2016




in magnitude to the 6.2 ppm obtained in the AOGCM study of Chikamoto et al. (2012). Fletcher et al. (2007) showed that most OGCMs in OCMIP-2 underestimate both the present-day outgassing of $CO_2$ in the high-latitude Southern Ocean by as much as 0.4 Pg C $yr^{-1}$ and the $CO_2$ uptake in the mid-latitude Southern Ocean by -0.2 Pg C $yr^{-1}$. Therefore, the true effect of sea ice changes in this region may have been larger than that modeled here. In particular, Brovkin et al. (2012) cited a 20 ppm sensitivity to SH sea ice after including increased diffusivity with their zonally-averaged ocean model.

### 3.4 Alkalinity response to ocean ventilation

Through a more vigorous ventilation of deep water, the $CO_2$ radiative forcing promoted a shift in the total DIC content (Fig. 6, discussed above) and alkalinity in the deep ocean (Fig. 8). These results are consistent with Galbraith et al. (2007), who documented a thorough ventilation of glacial deep waters in the North Pacific around 14500 BP, which coincided with a 10 ppm increase in atmospheric $CO_2$ in the ice core record. However, the replacement of glacial deep waters containing high levels of respired DIC with surface waters that have relatively low DIC and higher [$CO_3^{2-}$] would have contributed further to a long term increase in atmospheric $CO_2$ by supporting more $CaCO_3$ sedimentation, thereby decreasing net ocean alkalinity (Galbraith et al. 2007).

While alkalinity-induced changes in the $pCO_2$ of the oceans are not possible in the CA transient setup (by definition), the differences between the FC HW and CO2rad HW experiments help quantify this effect. The only distinction between these two simulations was the radiative forcing of $CO_2$ imposed on the CO2rad HW experiment. The FC HW run produced a slight increase in alkalinity between the LGM and the Holocene; carbonate compensation in favour of

Clim. Past Discuss., doi:10.5194/cp-2016-24, 2016
Manuscript under review for journal Clim. Past
Published: 17 March 2016




sediment burial was unable to outpace the weathering (alkalinity) inputs into the ocean until the late Holocene, contributing to the lower atmospheric $CO_2$ (~180-182 ppm) toward the end of the simulation. The CO2rad HW experiment showed the opposite trend, with a significant net decrease in alkalinity (40 μmol $kg^{-1}$, see Fig. 8a) and a pronounced increase in $CO_2$ to 215 ppm during the Holocene (Fig. 1a), outpacing the CO2rad CA simulation by 10 ppm by the mid-Holocene. This is aided by both a decrease in DIC content of the deep oceans due to greater ventilation (Fig. 6a-b) accompanied by a larger increase in precipitated calcite (Fig. 8c).

The alkalinity of the CO2rad HW and FC HW simulations began to diverge between 17000 BP and 16000 BP (Fig. 8a, purple line vs. orange line), coincident with the MOC recovery in the CO2rad simulations and reduced DIC storage in the deep Atlantic Ocean. This AMOC-induced change in alkalinity is portrayed by the average column depth-integrated alkalinity differences in Fig. 9a-b, which shows Atlantic waters losing alkalinity with time (consistent with the evolution discussed in Yu et al. 2014). Proxies tend to relate changes in alkalinity more specifically to [$CO_3^{2-}$] (for example, Catubig et al. (1998); Yu et al. (2014); Yu et al. (2010); Rickaby et al. (2010), and references therein), and subtracting alkalinity (Alk) from DIC in the model's spatial output allows a rough approximation of this quantity (Zeebe and Wolf-Gladrow 2001). By 9000 BP, the CO2rad HW simulation provides Δ[Alk-DIC] changes since the LGM below 2990 m of +26-42 μmol $kg^{-1}$ in the North Atlantic (above current estimates), +5-10 μmol $kg^{-1}$ in most of the Pacific (comparable to Yu et al. (2010)), little net change in the Southern Ocean, and -10 μmol $kg^{-1}$ in the Weddell Sea (below current estimates). A decrease in [Alk-DIC] in intermediate waters was also produced in the Atlantic (not shown), as in Yu et al. (2010).

Clim. Past Discuss., doi:10.5194/cp-2016-24, 2016
Manuscript under review for journal Clim. Past
Published: 17 March 2016




However, Fig. 9 shows that $[CO_3^{2-}]$ during deglaciation (Fig. 9c) and the early interglacial (Fig. 9d) was also greater in the CO2rad HW simulation compared to the neo-glacial FC HW simulation in the Atlantic, with much smaller changes in the Pacific. The contrast between the CO2rad HW and FC HW in the North Atlantic (+20 to +25μmol $kg^{-1}$) are similar to the +20 μmol $kg^{-1}$ LGM-to-Holocene change given in Yu et al. (2010), and the simulated change ( -24 μmol $kg^{-1}$) in the deep Weddell Sea is comparable to that given in Rickaby et al. (2010) ( -25 μmol $kg^{-1}$). Although the proxy record of glacial-interglacial changes in $[CO_3^{2-}]$ at sufficient resolution is highly limited and prevents firm conclusions, the spatial distribution in Fig. 10c-d agrees qualitatively with some evidence available to date. In other words, the $CO_2$-ventilation feedback causes changes in the alkalinity and DIC in the model ocean that match the sign and magnitude of the proxy-derived changes in $[CO_3^{2-}]$ in the deep Atlantic and Weddell Sea (Yu et al. 2010; Rickaby et al. 2010).

In the simulations considered here, however, deep ocean DIC changes were more pronounced in the Atlantic and Southern Indian than they are in the Pacific, which remains relatively poorly-ventilated until the mid-Holocene. This is in contrast to proxy evidence in Galbraith et al. (2007), which documented an important deglacial ventilation in the North Pacific starting around 14500 BP. As a consequence, the earlier real-world ventilation of Pacific DIC during the Bølling-Allerød would have led to an even greater long-term decrease in alkalinity than modelled here through enhanced sedimentation in the Pacific basin following the replacement of deep waters (Galbraith et al. 2007). The model did, in fact, slowly increase the circulation in CO2rad HW until a renewal of deep waters in the North Pacific was completed abruptly between 8000 BP and 6000 BP in a manner similar to that illustrated in Simmons et al. (2013). This Holocene renewal of deep Pacific waters also stimulated a further reduction in

Clim. Past Discuss., doi:10.5194/cp-2016-24, 2016
Manuscript under review for journal Clim. Past
Published: 17 March 2016




ocean alkalinity (Fig. 8a). The distribution of Antarctic marine ice shelves (the interpolated ICE-4G database) influenced the timing of the ventilation of North Pacific deep waters (see Simmons et al. 2013); an earlier ice shelf transition might force a more accurate North Pacific flush of DIC, which would in turn permit an earlier alkalinity-induced increase in atmospheric $CO_2$ during the Holocene. The ice configuration around Antarctica merits further study in this regard in order to determine whether there was a more abrupt and earlier ventilation of the North Pacific as proxy evidence suggests (Galbraith et al. 2007).

## 3.5 Sensitivity to Weathering and Carbonate Compensation

Another important factor affecting ocean alkalinity is the chemical weathering rate. Despite the model's inability to produce a deglacial increase in atmospheric $CO_2$ without $CO_2$ radiative forcing, it demonstrated significant sensitivity to the choice of weathering rate. The difference in weathering rate explains the approximately 10-15 ppm difference between the FC LW and FC HW simulations. Fig. 8a shows that the lower weathering rate is associated with a lowering of mean alkalinity (by -33 μmol $kg^{-1}$) and the higher weathering rate results in a net increase in alkalinity (by +10 μmol $kg^{-1}$). These findings may seem rather intuitive, but they demonstrate the relative importance of carbonate compensation, weathering, sedimentation flux, ocean ventilation, and deglacial atmospheric $CO_2$ changes.

A closer look at the FC LW simulation reveals that the sedimentation rate increased with time and exceeded the weathering rate for the entire simulation after 19000 BP (Fig. 8c, green line vs. light grey line), associated with an increase in calcifiers. Because sedimentation (an alkalinity sink) surpassed weathering (alkalinity source) for virtually the entire simulation, the greater removal of carbonate and bicarbonate in the surface ocean led to a downwelling of waters

Clim. Past Discuss., doi:10.5194/cp-2016-24, 2016
Manuscript under review for journal Clim. Past
Published: 17 March 2016




that have low [$CO_3^{2-}$], supporting a shallower lysocline and greater (oxic) dissolution of sediments and calcite rain. This is reflected in Fig. 8c, which shows that the FC LW sediment flux dipped below the FC CA sediment flux after 15000 BP.

The limited impact of carbonate compensation for the lower weathering rate is illustrated in Fig. 8d by changes in the CCD (defined here as the level where the rate of sedimentation equals the rate of dissolution). While the CCD was shallowest in the FC LW experiment compared to other runs, it still deepened during ventilations and did not rise above the original depth until 5500 BP. The rapid shoaling in the late Holocene appears to be aided by the increasing prevalence of more corrosive, high DIC southern-sourced deep waters after the Antarctic marine ice shelf disappearance (6000 BP-5000 BP) (Simmons et al. 2013). However, before this transition, a comparison of Fig. 8d with Fig. 5c reveals that the CCD deepening in the simulation was stimulated by greater ventilation (i.e., a stronger alkalinity pump to the deep ocean via the NADW). Although the partial recovery of the NADW driven by land ice and orbital forcing is much more limited without the addition of $CO_2$ radiative forcing, the somewhat more intense downwelling of low-DIC, high-alkalinity North Atlantic surface waters appears to be sufficient to support a deepening of the CCD. Without these changes in the MOC, a CCD shoaling would be supported throughout the simulation based on carbonate compensation. Therefore, a combination of low weathering (low alkalinity input), more calcite rain, and greater ventilation (which flushes deep DIC and lowers the CCD) helped drive down ocean alkalinity and supported a long-term increase in atmospheric $CO_2$.

The FC HW simulation shows a different pattern of carbonate compensation; from the beginning of the simulation to 11000 BP, the net sediment flux (Fig. 8c, purple line) remained below the weathering rate (Fig. 8c, dark purple line), and the greatest deepening of the CCD

Clim. Past Discuss., doi:10.5194/cp-2016-24, 2016
Manuscript under review for journal Clim. Past
Published: 17 March 2016




occurred during this time (Fig. 8d). In this case, the more intense ventilation after 16000 BP (Fig. 5c) and carbonate compensation (Fig. 8c) together favored a deepening of the CCD up to the beginning of the Holocene. This allowed for more sediment preservation and caused the sediment flux to drift above that of the FC CA simulation (Fig. 8b,c, blue line vs. purple line).Then after 11000 BP (approximately the beginning of the Holocene), the calcite flux surpassed the weathering rate, resulting in increasing dissolution with time by the mid-Holocene (in Fig. 8c, the purple line re-approaches blue line), although the long-term shoaling of the CCD associated with this effect (after 7000 BP) was nearly negligible (Fig. 8d). The deepening of the CCD accompanied by a larger sediment flux contributed to the decrease in alkalinity during the Holocene in this simulation, although this change is not substantial enough to counter the increase in ocean alkalinity during the late Pleistocene associated with a greater alkalinity source (weathering) than sink (sedimentation).

By contrast, when $CO_2$ radiative forcing was added to HW experiment, the sediment flux surpassed the weathering flux much earlier (16500 BP) and exceeded it by a much greater quantity ( 57 Tg C $yr^{-1}$) than in the simulation without radiative forcing (17 Tg C $yr^{-1}$). Correspondingly, the greater dissolution supported after 16500 BP drove the sediment flux significantly below the constant alkalinity experiment (CO2rad CA) after 11000 BP (Fig. 8c, light orange line vs. red line). Carbonate compensation in the CO2rad HW simulation should, in turn, support a more pronounced shoaling of the CCD than in the FC LW simulation (in which the sedimentation flux only surpassed weathering by a maximum of 29 Tg C $yr^{-1}$). However, the CCD in the CO2rad HW experiment remained below the original LGM level until 5000 BP and did not shoal above the FC LW CCD. The implication is that the greater ventilation stimulated by the $CO_2$-ventilation feedback, favouring the replacement of low-alkalinity, high-DIC deep

Clim. Past Discuss., doi:10.5194/cp-2016-24, 2016
Manuscript under review for journal Clim. Past
Published: 17 March 2016




waters with higher-alkalinity, lower-DIC surface waters, dominated the evolution of ocean alkalinity for most of the simulation.

These results are generally consistent with the proxy data presented in Yu et al. (2010), which suggest that abyssal oceans demonstrated a decrease in deep-ocean DIC content and increase in $[CO_3^{2-}]$ into the early Holocene in the deep Equatorial Pacific and North Atlantic in response to a ventilation of the deep ocean. Moreover, they support the conjecture in Rickaby et al. (2010) that, for a lower weathering rate for the LGM, an increase in sedimentation flux (due to a low CCD) can by itself work to decrease alkalinity and initiate an increase in $CO_2$. Our modeling results also suggest, however, that the same net effect (greater abyssal alkalinity and a deeper CCD) can be obtained from more ventilation of the deep ocean for both weathering rates, including in cases where carbonate compensation opposes the ventilation-induced alkalinity change. Further more, proxy records (Foster and Vance 2007; Vance et al. 2009; Crocket et al. 2012; Crocket et al. 2013) suggest that increased weathering flux into the North Atlantic coincides with periods of deeper overturning in the same region, which could accelerate deep sedimentation in NADW-dominated deep ocean basins more than modelled in the current study.

In summary, weathering dominated ocean alkalinity changes in our simulations, except in simulations with stronger, early deglacial deep-ocean ventilations. Greater ocean ventilation, in turn, had a more immediate impact on alkalinity than carbonate compensation, except for very long time scales (~15000-20000 years). Greater ocean alkalinity in the HW simulation drove $CO_2$ (180-182 ppm) slightly below the CA simulation (183 ppm), whereas the relatively higher end-result $CO_2$ (195 ppm) obtained in the LW simulation was driven by the reduction in ocean alkalinity due to lower alkalinity inputs. Only the larger ventilation change in the CO2rad HW (with intensified calcite sedimentation) led to an earlier downwelling of high-alkalinity surface

Clim. Past Discuss., doi:10.5194/cp-2016-24, 2016
Manuscript under review for journal Clim. Past
Published: 17 March 2016


Climate of the Past Discussions
Open Access
EGU

waters, which allowed greater deep sedimentation and a decrease in alkalinity. Given the enhanced ventilation of the $CO_2$ radiative forcing simulation, weathering would have to increase markedly for the oceans to be able to gain alkalinity as in the HW simulation.

### 3.6 The Alkalinity Response to Holocene Terrestrial Uptake

Broecker et al. (1999) proposed that terrestrial uptake during the early Holocene (boreal forests and expanded monsoonal vegetation) contributed to a deglacial-interglacial alkalinity change by sequestering $CO_2$ from the atmosphere and surface ocean, thus increasing the sea surface concentration of carbonate relative to dissolved $CO_2$. The downwelling of these low $pCO_2$, high [$CO_3^{2-}$] waters in the mid-Holocene would have deepened the CCD, allowing more sedimentation of falling $CaCO_3$ shells and ultimately reducing the [$CO_3^{2-}$] of the ocean. Broecker et al. (1999) documented the removal of alkalinity through the decrease in [$CO_3^{2-}$] from the size distribution of $CaCO_3$ shells in western tropical Atlantic and western tropical Pacific cores, which implied a late Holocene 11±2 μmol $kg^{-1}$decrease in [$CO_3^{2-}$] and over 20 ppm atmospheric $CO_2$ increase due to greater sedimentation during the early and mid-Holocene. In subsequent modelling studies, Joos et al. (2004) attributed 4-11 ppm of the Holocene $CO_2$ increase to an alkalinity decline in response to a sediment preservation event; Kleinen et al. (2010) argued that there was no significant difference due to this effect from sensitivity simulations including and excluding terrestrial changes, whereas Menviel and Joos (2012) attributed about +5.3 ppm in response to terrestrial uptake during the Holocene.

Of the results presented in this study, the PC HW simulation (Fig. 10a-b) provides the best illustration of this effect, as it imposes a decrease in atmospheric $CO_2$ (Supplementary Fig. 1a) between the early and mid-Holocene, as documented in the ice core record in Petit et al. (1999). This caused 125 Pg C to be extracted from the oceans (Supplementary Fig. 1b).

Clim. Past Discuss., doi:10.5194/cp-2016-24, 2016
Manuscript under review for journal Clim. Past
Published: 17 March 2016




However, the resulting total ocean alkalinity decrease of 4 μmol $kg^{-1}$ (Fig. 10a, pink line) could not account for the pace of the $CO_2$ increase after the mid-Holocene, requiring continued injections of carbon into the atmosphere in order to reproduce the late Holocene rise in $CO_2$. Fig. 10c-d show the change in the alkalinity and [Alk-DIC] patterns for the PC HW simulation between 7000 B.C and 5600 BP, just prior to the Antarctic ice shelf transition (occurring in the model at 5500 BP) and before renewed acidification from external $CO_2$ sources (Supplementary Fig. 1b). It shows the greatest alkalinity losses are in the Pacific Ocean (Fig. 12a), where deep Δ[Alk-DIC] is relatively high (Fig.12b), whereas a low [Alk-DIC] anomaly drove down deep ocean values in the Atlantic. The carbonate losses in the Atlantic had already begun by this date (-5 to -10 μmol $kg^{-1}$), whereas in the Pacific they had not yet been achieved (+5 μmol $kg^{-1}$). By 3000 BP (not shown), the low carbonate anomaly began to move to the Equatorial Pacific (-5 μmol $kg^{-1}$), whereas the Atlantic anomaly (-25 μmol $kg^{-1}$) was overestimated (due in part to the more prominent AABW after the aforementioned ice shelf transition).

Another approach to evaluating terrestrial-alkalinity interactions as proposed by Broecker et al. (1999) is to free the carbon cycle in the PC simulations after 8000 BP (i.e, following the extraction of DIC from the ocean). We did this for both the constant alkalinity experiment (PC CA, Fig. 11, dark blue line) and the higher weathering rate (PC HW, Fig. 11a, dark purple line) to isolate the effect of the alkalinity change on atmospheric $CO_2$. Fig. 11a shows that there is virtually no difference in the end-result atmospheric $CO_2$ concentrations for these two simulations (251.3 ppm). Furthermore, the alkalinity change following 6000 BP. in the freed PC HW simulation (Fig. 11b, dark purple line) is small (5 μmol $kg^{-1}$), becoming roughly constant after 6000 BP. Therefore, it appears that the greater downwelling of more corrosive Southern Ocean-generated waters in these simulations after 6000 BP exactly counterbalanced the slowly

Clim. Past Discuss., doi:10.5194/cp-2016-24, 2016
Manuscript under review for journal Clim. Past
Published: 17 March 2016




decreasing alkalinity in response to DIC removal between 10000 BP and 8000 BP, leading to unchanging alkalinity in the freed PC HW simulation. Redoing these two simulations (freed PC CA and freed PC HW) with more extensive ice shelves (Fig. 11b, light blue and light purple line respectively) as in Simmons et al. (2013) led to less AABW formation and a more prominent NADW. As Fig. 11b reveals, the more prominent NADW caused alkalinity to continue decreasing during the late Holocene in the PC HW simulation, allowing atmospheric $CO_2$ to be 10 ppm higher than in the PC HW simulation without ice shelves and 7 ppm higher than the constant alkalinity experiment with the same more-extensive ice shelves. The significantly greater atmospheric $CO_2$ concentrations in the PC HW simulation with Antarctic marine ice shelves suggests that a dominant NADW is required in order for ocean alkalinity to continue decreasing in response to the early Holocene terrestrial uptake. The mechanism proposed by Broecker et al. (1999) thus appears to be strongly dependent on the ocean circulation state and the proportion of AABW to NADW at depth in the model.

Results from the FC simulations also suggest a limited impact of the terrestrial uptake on ocean alkalinity without the inclusion of more extensive Antarctic ice shelves. Ciais et al. (2012) scaled back the terrestrial uptake to ~300 Pg C between the LGM to the pre-industrial Holocene, which is only slightly greater than the ~200-250 Pg C terrestrial uptake between the early and late Holocene in our FC and CO2rad simulations. The FC HW simulation, which experienced a terrestrial uptake of ~130 Pg C between 14500 BP and 8000 BP (Fig. 1c), induced a slight decrease in alkalinity into the later Holocene (Fig. 8a, purple line), although a significant fraction of this signal seems to be associated with more ventilation (Fig. 5c) and calcite rain (Fig. 8c) during this time period. While terrestrial uptake in our simulations has a limited impact on interglacial alkalinity, the CO2rad results do provide for a substantial alkalinity-induced increase

Clim. Past Discuss., doi:10.5194/cp-2016-24, 2016
Manuscript under review for journal Clim. Past
Published: 17 March 2016




in atmospheric $CO_2$ during the Holocene in the CO2rad HW simulation. Furthermore, this increase occurred in spite of decreased vegetation carbon storage between the LGM and the early Holocene. In particular, the terrestrial carbon storage in the CO2rad HW scenario (with higher $CO_2$) only began to (slowly) surpass the FC HW simulation at ~9500 BP and was only 20 Pg C larger than the FC HW simulation at 8000 BP, at which point (comparing the CO2rad CA and CO2rad HW trends in Fig. 1a) the alkalinity-induced increase in atmospheric $CO_2$ in the CO2rad HW simulation was already well underway. A general decrease in $[CO_3^{2-}]$ over the course of the late Holocene was also obtained in this experiment (Fig. 12a,b), again perhaps somewhat overestimated due to the influence of the Antarctic ice shelf transition on AABW but also on the scale of the changes given in Broecker et al. (1999). Thus, in our results, the effects of the greater ocean ventilation of respired deep-ocean DIC (the $CO_2$-ventilation feedback) appears to be the more prominent factor in promoting a decrease in ocean alkalinity.

# 4 Conclusions

In this paper, we presented a suite of simulations using the UVic ESCM v. 2.9 to test the model's transient response to land ice changes, orbital parameter changes, $CO_2$ radiative forcing, and alkalinity inputs (from different constant weathering rates) from the LGM to the present. In the simulations without high latitude terrestrial carbon storage, we focused on important oceanic processes. These simulations failed to reproduce the full deglacial rise in atmospheric $CO_2$. Depending on the processes included, we simulated both a decline in atmospheric CO2 of ~10 ppm to an increase of up to 25 ppm. Modeling experiments with only Milankovitch and ice sheet forcing did not produce a full recovery in the Atlantic meridional overturning circulation, leading to higher oceanic carbon storage and the lowest values of atmospheric $CO_2$ (unchanged or lower than the LGM value, depending on the weathering rate). Those modeling experiments that

Clim. Past Discuss., doi:10.5194/cp-2016-24, 2016
Manuscript under review for journal Clim. Past
Published: 17 March 2016




included $CO_2$ radiative forcing produced a warmer ocean, a more thorough ventilation of the deep ocean. This suggests that the warming effect provided by higher atmospheric $CO_2$ acts as a positive feedback on the deglacial rise in $CO_2$.

This $CO_2$-ventilation feedback occurred in the model in response to stronger overturning circulation in the North Atlantic and greater outgassing in the Southern Ocean, both enhanced by reduced sea ice extent. This ventilation of deep-ocean DIC allowed atmospheric $CO_2$ to increase by ~10 ppm. The alkalinity decrease in the ocean in response to greater ventilation contributed an additional 10 ppm in our simulations, mostly over the course of the late deglacial and interglacial periods due to the downwelling of high-alkalinity, low-DIC waters in the North Atlantic. These circulation features are largely driven by a reorganization of the Atlantic and Indian oceans, where the NADW has more influence in the model. In terms of alkalinity changes, a comparison with simulations without $CO_2$ radiative forcing reveals that the $CO_2$-ventilation feedback in the model may by itself potentially explain deep ocean variations in $[CO_3^{2-}]$ on the order of those given in Yu et al. (2010) and Rickaby et al. (2010) in the deep Atlantic and Weddell Sea.

The ocean alkalinity and atmospheric $CO_2$ during deglaciation are also strongly influenced by weathering. When only ice sheets and Milankovitch forcing are prescribed, the total ocean alkalinity was largely driven by the weathering rate, with higher (lower) weathering rates leading to greater (less) ocean alkalinity and lower (higher) atmospheric $CO_2$. Only the thorough, early ventilation of deep-ocean DIC that occurred in the $CO_2$ radiative forcing experiments were able to produce a net lowering of total ocean alkalinity under higher weathering rates. This alkalinity decrease occurred in response to a lower CCD in the Atlantic, Indian, and South Pacific basins in response to stronger NADW formation and overturning. The

Clim. Past Discuss., doi:10.5194/cp-2016-24, 2016
Manuscript under review for journal Clim. Past
Published: 17 March 2016




results suggest that an early ventilation event is important for stimulating a decrease in alkalinity during the deglacial and interglacial periods to maintain higher atmospheric $CO_2$. However, the constant weathering rates used for this experiment assume an equilibrium between weathering and sedimentation for two different points during the late glacial period (23000 BP and 21000 BP). Rickaby et al. (2010), on the other hand, suggested that the weathering rate may have been substantially lower than the sedimentation rate during the LGM. This would have resulted in an increased atmospheric $CO_2$ during the early deglacial period. While the present set of simulations do not model this differentiation in weathering and sedimentation rates during the LGM and early deglacial, they support the hypothesis that lower weathering rates and greater deep ocean ventilation worked together to allow a net decrease in alkalinity.

In summary, our results suggest that there are potential oceanic contributors to the atmospheric $CO_2$ rise during deglaciation:

(1) Lower weathering rates during the early deglacial maintained a slowly increasing atmospheric $CO_2$ (providing that the sedimentation rate exceeded the weathering rate).

(2) Ventilations of glacial deep water, the reinvigoration of the NADW, and stronger overturning supported an outgassing of respired $CO_2$ from the deep ocean.

(3) The ventilation of high-$CO_2$ deep waters and replacement with surface waters with higher carbonate concentrations allowed alkalinity to continue to decrease (through greater sedimentation) in the late deglacial and early interglacial period, maintaining the initial increases in $CO_2$ even for higher weathering rates.

The three steps together did not account for the full deglacial rise in $CO_2$ in the simulations presented here. This is likely due to the fact that our experimental setup does not account for

Clim. Past Discuss., doi:10.5194/cp-2016-24, 2016
Manuscript under review for journal Clim. Past
Published: 17 March 2016




several important processes. In particular, during our equilibrium simulation for the LGM, we removed 366 Pg C of terrestrial carbon from the pre-industrial spin-up that would have otherwise been transferred under the ice sheet. Reconfiguring the model to reapportion this carbon to the oceans and terrestrial biosphere (under fixed $CO_2$) during the equilibrium simulation would have increased the DIC content of the oceans and enhanced the ventilation-alkalinity response during deglaciation. Furthermore, the downwelling of $CO_2$ would have increased sediment dissolution and provided an even lower equilibrium weathering rate than the HW and LW rates used here. Huiskamp and Meissner (2012) found that the upwelling of DIC in their simulations for the Mystery Interval could only explain ~58% of the $CO_2$ rise through ocean processes, perhaps also because of the lack of transfer of terrestrial carbon to the deep ocean in these experiments. A weakened biological pump during NADW shutdowns (with less calcite rain and sedimentation as a result) would also lead to an increase in alkalinity, and thus greater oceanic absorption of atmospheric $CO_2$. Our results thus indicate that a combination of a lower weathering rate and higher initial DIC content of the oceans could allow for a larger early deglacial increase in atmospheric $CO_2$ than in the present simulations.

Terrestrial processes also provided important contributions to the simulated deglacial and interglacial carbon cycle. Experiments with only $CO_2$ radiative forcing, ice sheet, and orbital changes produced modest (200-250 Pg C) increases in terrestrial carbon storage from the LGM to the present. Increasing land availability and warmer temperatures were not sufficient mechanisms to stimulate net gains in vegetation carbon, as the lower $CO_2$ levels (and limited fertilization) led to carbon losses in the tropics and subtropics that compensated for greater carbon sequestration at higher latitudes. Simulations with prescribed $CO_2$, in which enough carbon was physically injected into the modeled Earth system to allow $CO_2$ to follow the ice core

Clim. Past Discuss., doi:10.5194/cp-2016-24, 2016
Manuscript under review for journal Clim. Past
Published: 17 March 2016




trend, produced an increase in terrestrial carbon storage of 600 Pg C, comparable to other recent modeling estimates (Prentice et al. 2011). Therefore, our simulations suggest that $CO_2$ fertilization accounts for most of the net vegetation carbon uptake since the LGM. Furthermore, this fertilization effect (when compared to the low fertilization simulations) provided a significant increase in temperatures (0.1-0.3°C) in the tropics and may have strengthened outgassing by warming important upwelling regions and increasing the baroclinic gradient (wind speeds) and coastal upwelling in the subtropics. The introduction of these temperature anomalies into a model with a three-dimensional atmosphere would go further in determining the importance of these fertilization-induced wind anomalies and would be a worthwhile endeavor for future work.

# Acknowledgements

The above work has been supported by the Natural Sciences and Engineering Research Council (NSERC) of Canada through discovery grants given to H. Damon Matthews and Lawrence A. Mysak, with additional funding from the Global Environmental and Climate Change Centre (GEC3). We also gratefully acknowledge Katrin Meissner, Eric Galbraith, and Marc-Olivier Brault for their invaluable suggestions and input in the preparation of this paper.

# References

Adkins JF, McIntyre K, Schrag DP (2002). The salinity, temperature, and $\delta^{18}O$ of the glacial deep ocean. *Science*, 298: 1769-1773.

Anderson RF, Ali S, Bradtmiller LI, Nielsen SHH, Fleisher MQ, Anderson BE, Burckle LH (2009) Wind-driven upwelling in the Southern Ocean and the deglacial rise in atmospheric $CO_2$. *Science*, 323: 1443-1448.

Archer DE (1996) A data-driven model of the global calcite lysocline. *Global Biogeochemical Cycles*, 10: 511-526.

Broecker WS, Yu J, Putnam AE (2015) Two contributors to the glacial $CO_2$ decline. *Earth and Planetary Science Letters*, 429: 191-196.

Clim. Past Discuss., doi:10.5194/cp-2016-24, 2016
Manuscript under review for journal Clim. Past
Published: 17 March 2016


Climate of the Past Discussions
Open Access
EGU

Broecker WS, Clark E, McCorkle DC, Peng T-H, Hajdas I, Bonani G (1999) Evidence for a reduction in the carbonate ion content of the deep sea during the course of the Holocene. *Paleoceanography*, 14: 744-752.

Broecker WS, Henderson GM (1998) The sequence of events surrounding Termination II and their implications for the cause of glacial-interglacial $CO_2$ changes. *Paleoceanography*, 13: 352-364.

Brovkin V, Brücher T, Kleinen T, Zaehle S, Joos F, Roth R, Spahni R, Schmitt J, Fischer H, Leuenberg M, Stone EJ, Ridgwell A, Chappellaz J, Kehrwald N, Barbane C, Blunier T, Jensen DD (2016) Comparative carbon cycle dynamics of the present and last interglacial. *Quaternary Science Reviews*, 137: 15-32.

Brovkin V, Ganopolski A, Archer D, Munhoven G (2012) Glacial $CO_2$ cycle as a succession of key physical and biogeochemical processes. *Climate of the Past*, 8: 251-264.

Catubig NR, Archer DE, Francois R, deMonocal P, Howard W, Yu E-F (1998) Global deep-sea burial rate of calcium carbonate during the last glacial maximum. *Paleoceanography*, 13: 298-310.

Ciais P, Tagliabue A, Cuntz M, Bopp L, Scholze M, Hoffmann G, Lourantou A, Harrison SP, Prentice IC, Kelley DI, Koven C, Piao SL (2012) Large inert carbon pool in the terrestrial biosphere during the Last Glacial Maximum. *Nature Geoscience*, 5: 74-79.

Chickamoto MO, Abe-Ouchi A, Oka A, Ohgaito R, Timmermann A (2012) Quantifying the ocean's role in glacial $CO_2$ reductions. *Climate of the Past*, 8: 545-563.

Claussen M, Mysak LA, Weaver AJ, Crucifix M, Fichefet T, Loutre MF, Weber SL, Alcamo J, Alexeev VA, Berger A, Calov R, Ganopolski A, Goosse H, Lohmann G, Lunkeit F, Mokhov II, Petoukhov V, Stone P, Wang Z (2002) Earth system models of intermediate complexity: Closing the gap in the spectrum of climate system models. *Climate Dynamics*, 18: 579-586.

Cox PM (2001) Description of the 'TRIFFID' dynamic global vegetation model. Hadley Centre Technical Note 24 pp. 1-16. Berks, UK: UK Met Office.

Cox PM, Betts RA, Bunton CB, Essery RLH, Rowntree PR, Smith J (1999) The impact of new land surface physics on the GCM simulation of climate and climate sensitivity. *Climate Dynamics*, 15**:** 183–203.

Crocket KC, Vance D, Foster GL, Richards DA, Tranter M (2012) Continental weathering fluxes during the last glacial/interglacial cycle: Insights from the marine sedimentary Pb isotope record at Orphan Knoll, NW Atlantic. *Quaternary Science Reviews*, 38: 89-99.

Clim. Past Discuss., doi:10.5194/cp-2016-24, 2016
Manuscript under review for journal Clim. Past
Published: 17 March 2016


Climate of the Past Discussions
Open Access
EGU

D'Orgeville M, Sijp WP, England MH, Meissner KJ (2010) On the control of glacial-interglacial atmospheric $CO_2$ variations by the Southern Hemisphere westerlies. *Geophysical Research Letters*, 37: L21703, doi:10.1029/2010GL045261.

Duplessy J-C, Labeyrie L, Waelbroeck C (2002) Constraints on the ocean oxygen isotopic enrichment between the Last Glacial Maximum and the Holocene: Paleoceanographic implications. *Quaternary Science Reviews*, 21: 315-330.

Eby M, Zickfeld K, Montenegro A, Archer D, Meissner KJ, Weaver AJ (2009) Lifetime of anthropogenic climate change: Millennial time scales of potential $CO_2$ and surface temperature perturbations. *Journal of Climate*, 22: 2501-2511.

Etheridge, DM, Steele, LP, Langenfelds, RL, Francey, RJ, Barnola, JM, and Morgan, VI. (1996) Natural and anthropogenic changes in atmospheric $CO_2$ over the last 1000 years from air in Antarctic ice and firn. Journal of Geophysical Research, 101: 4115–4128.

Ewen TL, Weaver AJ, Eby M (2004) Sensitivity of the inorganic ocean carbon cycle to future climate warming in the UVic coupled model. *Atmosphere Ocean*, 42: 23-42.

Fanning AE, Weaver AJ (1996) An atmospheric energy-moisture balance model: Climatology, interpentadal climate change, and coupling to an ocean general circulation model. *Journal of Geophysical Research*, 101: 15111-15128.

Fletcher SEM, Gruber N, Jacobson AR, Gloor M, Doney SC, Dutkiewicz S, Gerber M, Follows M, Joos F, Lindsay K, Menemenlis D, Mouchet A, Müller SA, Sarmiento JL (2007) Inverse estimates of the oceanic sources and sinks of natural CO2 and the implied oceanic transport. *Global Biogeochemical Cycles*, 21: GB1010, doi:10.1029/2006GB002751.

Foster GL, Vance D (2006) Negligible glacial-interglacial variation in continental chemical weathering rates. *Nature*, 444: 918-921.

Galbraith ED, Jaccard SL, Pedersen TF, Sigman DM, Haug GH, Cook M, Southon JR, Francois R (2007) Carbon dioxide release from the North Pacific abyss during the last deglaciation. *Nature*, 449: 890-893.

Galbraith ED, Jaccard SL (2015). Deglacial weakening of the oceanic soft tissue pump: global constraints from sedimentary nitrogen isotopes and oxygenation proxies. *Quaternary Science Reviews*, *109*, 38-48.

Gent PR, McWilliams JC (1990) Isopycnal mixing in ocean circulation models. *Journal of Physical Oceanography*, 20: 150– 155.

Gersonde R, Crosta X, Abelmann A, Armand L (2005) Sea-surface temperature and sea ice distribution of the Southern Ocean at the EPILOG Last Glacial Maximum—a circum-

Clim. Past Discuss., doi:10.5194/cp-2016-24, 2016
Manuscript under review for journal Clim. Past
Published: 17 March 2016


Climate of the Past Discussions
Open Access
EGU

Antarctic view based on siliceous microfossil records. *Quaternary Science Reviews*, 24: 869-896.

Hodell DA, Venz KA, Charles CD, Ninnemann US (2003) Pleistocene vertical carbon isotope and carbonate gradients in the South Atlantic sector of the Southern Ocean. *Geochemistry, Geophysics, Geosystems*, 4: 1004, doi:10.1029/2002GC000367.

Huiskamp WN, Meissner KJ (2012) Oceanic carbon and water masses during the Mystery Interval: A model-data comparison study. *Paleoceanography*, 27, PA4206, doi:10.1029/

Huybers P, Langmuir C (2009) Feedback between deglaciation, volcanism, and atmospheric $CO_2$. *Earth and Planetary Science Letters*, 286: 479-491.

Indermühle A, Stocker TF, Joos F, Fischer H, Smith H, Wahlen M, Deck B, Mastroianni D, Tschumi J, Blunier T, Meyer R, Stauffer B (1999) Holocene carbon-cycle dynamics based on $CO_2$ trapped in ice at Taylor Dome, Antarctica. *Nature*, 398: 121-126.

Jaccard SL, Galbraith ED, Sigman DM, Huag GH, Francois R, Pedersen TF, Dulski P, Thierstein HR (2009) Subarctic Pacific evidence for a glacial deepening of the oceanic respired carbon pool. *Earth and Planetary Science Letters*, 277: 156-166.

Jolly D, Haxeltine A (1997) Effect of low glacial atmospheric $CO_2$ on tropical African montane vegetation. *Science*, 276:786-788.

Joos, F, Gerber, S, and Prentice, IC (2004) Transient simulations of Holocene atmospheric carbon dioxide and terrestrial carbon since the Last Glacial Maximum. *Global Biogeochemical Cycles*, 18, doi:10.1029/ 2003GB002156.

Kalnay E, Kanamitsu M, Kistler R, Collins W, Deaven D, Gandin L, Iredell M, Saha S, White G, Woollen J, Zhu Y, Chelliah M, Ebisuzaki W, Higgins W, Janowiak J, Mo KC, Ropelewski C, Wang J, Leetma A, Reynolds R, Jenne R, Joseph D (1996) The NCEP/NCAR 40-year reanalysis project. *Bulletin of the American Meteorological Society*, 77: 437-471.

Kleinen T, Brovkin V, von Bloh W, Archer D, Munhoven G (2010) Holocene carbon cycle dynamics, *Geophysical Research Letters*, 37, L02705, doi:10.1029/2009GL041391.

Kohfeld KE, Ridgwell A (2009) Glacial-interglacial variability in atmospheric $CO_2$. In *Surface Ocean-Lower Atmosphere Processes*, Geophysical Research Series 37, Washington DC: American Geophysical Union, p.251–286, doi: 10.1029/2008GM000845.

Köhler P, Knorr G, Bard E (2014) Permafrost thawing as a possible source of abrupt carbon release at the onset of the Bølling/Allerød. *Nature Communications*, 5. doi: 10.1038/ncomms5520.

Clim. Past Discuss., doi:10.5194/cp-2016-24, 2016
Manuscript under review for journal Clim. Past
Published: 17 March 2016


Climate of the Past Discussions
Open Access
EGU

Lambert F, Delmonte B., Petit JR, Bigler M, Kaufmann PR, Hutterli MA, Stocker TF, Ruth U, Steffensen JP, Maggi V (2008) Dust-climate couplings over the past 800,000 years from the EPICA Dome C ice core. *Nature*, 452: 616-619.

Lamy F, Hebbeln D, Röhl U, Wefer G (2001) Holocene rainfall variability in southern Chile: A marine record of latitudinal shifts of the Southern Westerlies. *Earth and Planetary Science Letters*, 18: 369-382.

Lupker M, France-Lanord C, Galy V, Lavé J, Kudrass H (2013) Increasing chemical weathering in the Himalayan system since the Last Glacial Maximum. *Earth and Planetary Science Letters*, 365: 243-252.

Marcott SA, Bauska TK, Buizert C, Steig EJ, Rosen JL, Cuffey KM, Fudge TJ, Severinghaus JP, Ahn J, Kalk ML, McConnell JR, Sowers T, Taylor KC, White JWC, Brook EJ (2014) Centennial-scale changes in the global carbon cycle during the last deglaciation. *Nature*, 514(7524), 616-619.

Marson JM, Wainer I, Matta MM, Liu Z (2014) The impacts of deglacial meltwater forcing on the South Atlantic Ocean deep circulation since the Last Glacial Maximum. *Climate of the Past*, 10, 1723-1734.

Matthews HD, Weaver AJ, Meissner KJ, Gillett NP, Eby M (2004) Natural and anthropogenic climate change: Incorporating historical land cover change, vegetation dynamics and the global carbon cycle. *Climate Dynamics*, 22: 461-479.

McManus JF, Francois R, Gherardi JM, Keigwin LD, Brown-Leger S (2004) Collapse and rapid resumption of Atlantic meridional circulation linked to deglacial climate changes. *Nature*, 428: 834-837.

Meissner KJ, Weaver AJ, Matthews HD, Cox PM (2003) The role of land-surface dynamics in glacial inception: A study with the UVic Earth System Model. *Climate Dynamics*, 21: 515-537.

Menviel L, Joos F (2012) Toward explaining the Holocene carbon dioxide and carbon isotope records: Results from transient ocean carbon cycle-climate simulations. *Paleoceanography*, 27: PA1207, doi:10.1029/2011PA002224.

Menviel L, Joos F, Ritz SP (2012) Simulating atmospheric $CO_2$, $^{13}C$ and the marine carbon cycle during the Last Glacial-Interglacial cycle: possible role for a deepening of the mean remineralization depth and an increase in the oceanic nutrient inventory. *Quaternary Science Reviews*, 56: 46-68.

Monnin E, Indermühle A, Dallenbach A, Flückiger J, Stauffer B, Stocker TF, Raynaud D, Barnola, J-M (2001) Atmospheric concentrations over the Last Glacial Termination. *Science*, 291: 112-114.

Clim. Past Discuss., doi:10.5194/cp-2016-24, 2016
Manuscript under review for journal Clim. Past
Published: 17 March 2016


Climate of the Past Discussions
Open Access
EGU

Montenegro A, Eby M, Kaplan JO, Meissner KJ, Weaver AJ (2006) Carbon storage on exposed continental shelves during the glacial-interglacial transition. *Geophysical Research Letters*, 33: L08703, doi:10.1029/2005GL025480.

Pacanowski RC (1995) MOM 2 documentation, user's guide and reference manual. *GFDL Ocean Group Technical. Rep*ort, Princeton, NJ: NOAA, GFDL.

Parekh P, Joos F, Müller SA (2008) A modeling assessment of the interplay between aeolian iron fluxes and iron-binding ligands in controlling carbon dioxide fluctuations during Antarctic warm events. *Paleoceanography*, 23: PA4202, doi:10.1029/2007PA001531.

Peltier WR (2002) Global glacial isostatic adjustment: Palaeogeodetic and space-geodetic tests of the ICE-4G (VM2) model. *Journal of Quaternary Science*, 17: 491-510.

Peterson CD, Lisiecki LE, Stern JV (2014) Deglacial whole-ocean $\delta^{13}C$ change estimated from 480 benthic foraminiferal records. *Paleoceanography*, 29: 549-563.

Petit JR, Jouzel J, Raynaud D, Barkov NI, Barnola J-M, Basile I, Bender M, Chappellaz J, Davis M, Delaygue G, Delmotte M, Kotlyakov VM, Lipenkov V, Lorius C, Pepin L, Ritz C, Saltzman E, Stievenard M (1999) Climate and atmospheric history of the last 420,000 Years from the Vostok ice core, Antarctica. *Nature*, 399: 429-436.

Prentice IC, Harrison SP, Bartlein PJ (2011) Global vegetation and terrestrial carbon cycle changes after the last ice age. *New Phytologist*, 189: 988-998.

Prentice IC, Harrison SP (2009) Ecosystem effects of $CO_2$ concentration: Evidence from past climates. *Climate of the Past*, 5: 297-307.

Rickaby RE, Elderfield H, Roberts N, Hillenbrand C-D, Mackensen A (2010) Evidence for elevated alkalinity in the glacial Southern Ocean. *Paleoceanography*, 25, PA1209, doi:10.1029/2009PA001762.

Ridgwell AJ, Watson AJ, Maslin MA, Kaplan J (2003) Implications of coral reef buildup for the controls on atmospheric $CO_2$ since the Last Glacial Maximum. *Paleoceanography*, 18, doi:10.1029/2003PA000893.

Ridgwell AJ (2003) An end to the "rain ratio" reign? *Geochemistry, Geophysics, Geosystems*, 4, doi:10.1029/2003GC000512.

Roche DM, Crosta X, Renssen H (2012) Evaluating Southern Ocean sea-ice for the Last Glacial Maximum and pre-industrial climates: PMIP-2 models and data evidence. *Quaternary Science Reviews*, 56: 99-106.

Roth, R, Joos F (2012) Model limits on the role of volcanic carbon emissions in regulating glacial–interglacial $CO_2$ variations. *Earth and Planetary Science Letters*, 329, 141-149.

Clim. Past Discuss., doi:10.5194/cp-2016-24, 2016
Manuscript under review for journal Clim. Past
Published: 17 March 2016


Climate of the Past Discussions
Open Access
EGU

Ruddiman WF, Kutzbach JE, Vavrus SJ (2011) Can natural or anthropogenic explanations of late-Holocene $CO_2$ and $CH_4$ increases be falsified? *The Holocene*, 21, 865-887.

Schartau M, Oschlies A (2003) Simultaneous data-based optimization of a 1d-ecosystem model at three locations in the North Atlantic: I. Method and parameter estimates. *Journal of Marine Research*, 61: 765–793.

Schmittner A, Oschlies A, Matthews HD, Galbraith ED (2008) Future changes in climate, ocean circulation, ecosystems, and biogeochemical cycling simulated for a business-as-usual CO2 emission scenario until year 4000 AD. *Global Biogeochemical Cycles*, 22: GB1013, doi:10.1029/2007GB002953.

Schmittner A, Galbraith ED (2008) Glacial greenhouse-gas fluctuations controlled by ocean circulation changes. *Nature*, 456: 373-376.

Schmittner A, Galbraith ED, Hostetler SW, Pederson TF, Zhang R (2007) Large fluctuations of dissolved oxygen in the Indian and Pacific oceans during Dansgaard-Oeschger oscillations caused by variations of North Atlantic Deep Water subduction. *Paleoceanography*, 22: PA3207, doi:10.1029/2006PA001384.

Schmittner A, Oschlies A, Giraud X, Eby M, Simmons HL (2005) A global model of the marine ecosystem for long-term simulations: Sensitivity to ocean mixing, buoyancy forcing, particle sinking, and dissolved organic matter cycling. *Global Biogeochemical Cycles*, 19: GB3004:1-17.

Simmons CT, Matthews HD, Mysak LA (2015). Deglacial climate, carbon cycle and ocean chemistry changes in response to a terrestrial carbon release. *Climate Dynamics*, doi: 10.1007/s00382-015-2646-6.

Simmons CT, Mysak LA, Matthews HD (2013) Investigation of the natural carbon cycle since 6000 BC using an intermediate complexity model: The role of Southern Ocean ventilation and marine ice shelves. *Atmosphere-Ocean*, 51: 187-212.

Stephens BB, Keeling RF (2000) The influence of Antarctic sea ice on glacial-interglacial variations. *Nature*, 404: 171-174.

Street-Perrot FA, Huang Y, Perrott RA, Eglinton G, Barker P, Khelifa LB, Harkness DD, Olago DO (1997) Impact of lower atmospheric carbon dioxide on tropical mountain ecosystem.

Thompson LG, Davis ME, Mosley-Thompson E, Sowers TA, Henderson KA, Zagorodnov S, Lin P-N, Mikhalenko VN, Campen RK, Bolzan JF, Cole-Dai J, Francou B (1998) A 25,000-year tropical climate history from Bolivian ice cores. *Science*, 282: 1858-1864.

Clim. Past Discuss., doi:10.5194/cp-2016-24, 2016
Manuscript under review for journal Clim. Past
Published: 17 March 2016


Climate of the Past Discussions
Open Access
EGU

Toggweiler JR, Russell JL, Carson SR (2006) Midlatitude westerlies, atmospheric $CO_2$, and climate change during the ice ages. *Paleoceanography*, 21: PA2005, doi:10.1029/2005PA001154.

Watson AJ, Naveira Garabato (2006) The role of Southern Ocean mixing and upwelling in glacial-interglacial atmospheric $CO_2$ change. *Tellus*, 58B, 73-87.

Weaver AJ, Eby M, Wiebe EC, Bitz CM, Duffy PB, Ewen TL, Fanning AF, Holland MM, MacFadyen A, Matthews HD, Meissner KJ, Saenko O, Schmittner A, Wang H, Yoshimori M (2001) The UVic Earth System Climate Model: Model description, climatology, and applications to past, present and future climates. *Atmosphere-Ocean*, 39: 361-428.

Yu J, Anderson RF, Rohling EJ (2014). Deep Ocean Carbonate Chemistry and Glacial-Interglacial Atmospheric $CO_2$ Changes. *Oceanography*, 27: 16-25.

Yu J, Broecker WS, Elderfield H, Jin Z, McManus J, Zhang F (2010). Loss of carbon from the deep sea since the Last Glacial Maximum. *Science,* 330:1084-1087.

Yu ZC (2011) Holocene carbon flux histories of the world's peatlands: Global carbon cycle implications. *The Holocene*, 21:761-774.

Zeebe RE, Wolf-Gladrow DA (2001) CO2 in seawater: equilibrium, kinetics, isotopes (Vol. 65). Gulf Professional Publishing.

Zech R (2012) A permafrost glacial hypothesis – Permafrost carbon might help explaining the Pleistocene ice ages, *Quaternary Science Journal*, 61 : 84–92.

Clim. Past Discuss., doi:10.5194/cp-2016-24, 2016
Manuscript under review for journal Clim. Past
Published: 17 March 2016


Climate of the Past Discussions
Open Access
EGU

# Figures

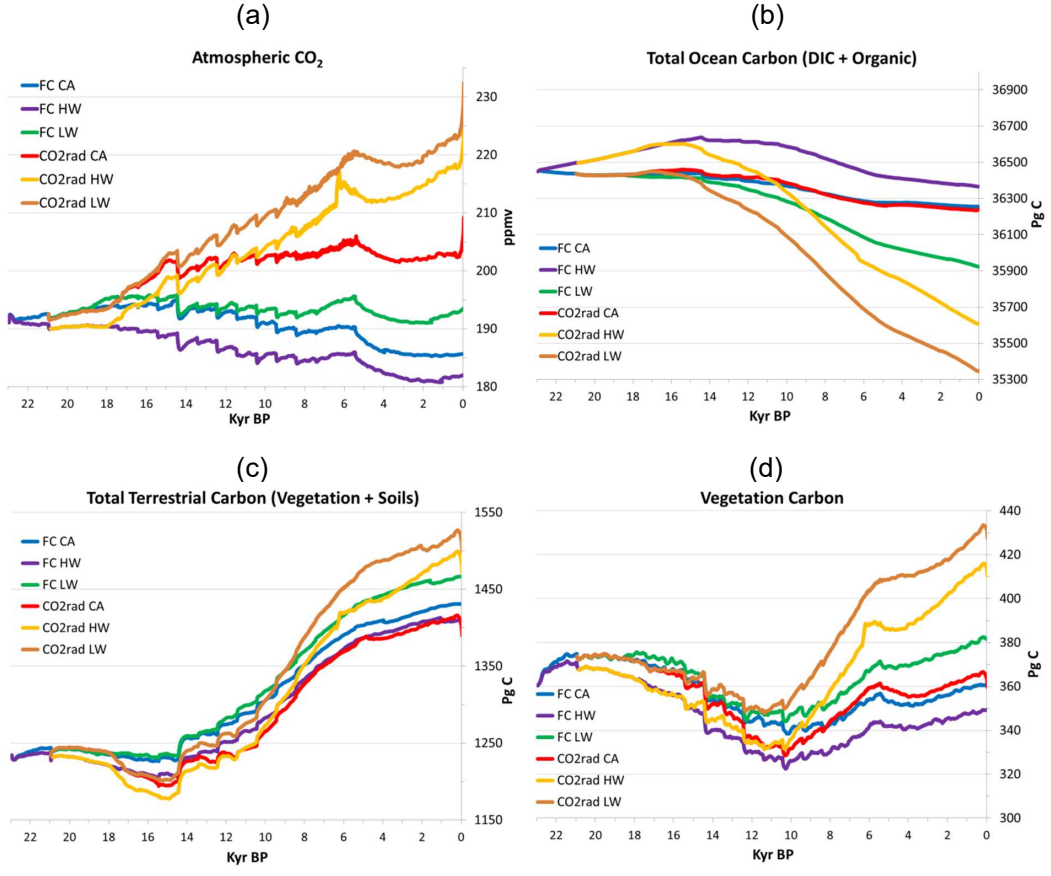


*Fig. 1: Carbon reservoirs that exchange directly with the atmosphere. These include (a) atmospheric carbon dioxide (ppmv), (b) total ocean carbon (organic and inorganic carbon), (c) total terrestrial carbon (both vegetation and soils), and (d) vegetation (above-ground) carbon. All simulations represented in this figure have a freely-evolving carbon cycle. They include separate transient simulations with constant ocean alkalinity (FC CA, blue line), a higher (12 Tmol $yr^{-1}$) constant weathering rate (FC HW, purple line), and a lower (10.1 Tmol $yr^{-1}$) constant weathering rate (FC LW, green line). These three simulations were repeated with $CO_2$ radiative forcing (denoted by warmer colours): CO2rad CA (red line), CO2rad HW (orange line), and CO2rad LW (tan line).*

Clim. Past Discuss., doi:10.5194/cp-2016-24, 2016
Manuscript under review for journal Clim. Past
Published: 17 March 2016


Climate of the Past
Discussions
Open Access
EGU

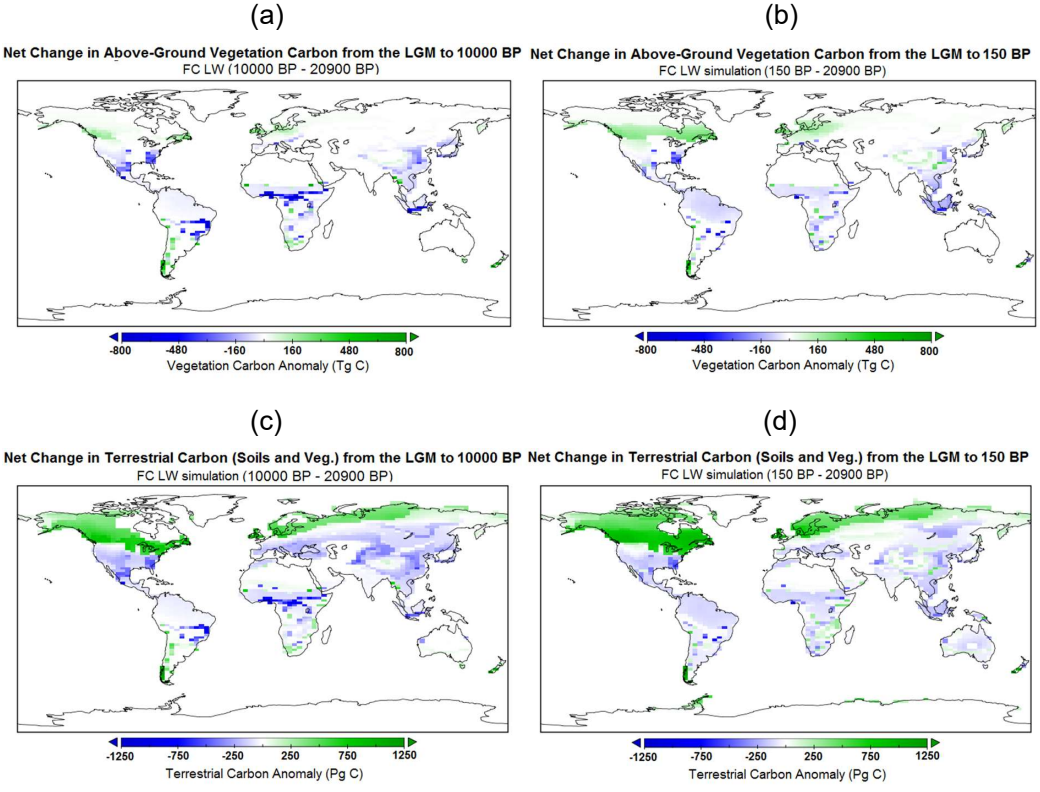


*Fig. 2: The net change in the spatial distribution of above-ground vegetation carbon at (a) 10000 Before Present (BP) and (b) 150 BP, and the net change in total terrestrial carbon (vegetation and soils) at (c) 10000 BP and (d) 150 BP since the LGM climate (defined as 20900 BP) for the FC LW simulation. Vegetation carbon anomalies are plotted on a scale of -800 Tg C to +800 Tg C, whereas terrestrial carbon anomalies are plotted from -1250 Tg C to +1250 Tg C.*

Clim. Past Discuss., doi:10.5194/cp-2016-24, 2016
Manuscript under review for journal Clim. Past
Published: 17 March 2016


Climate of the Past
Discussions
Open Access
EGU

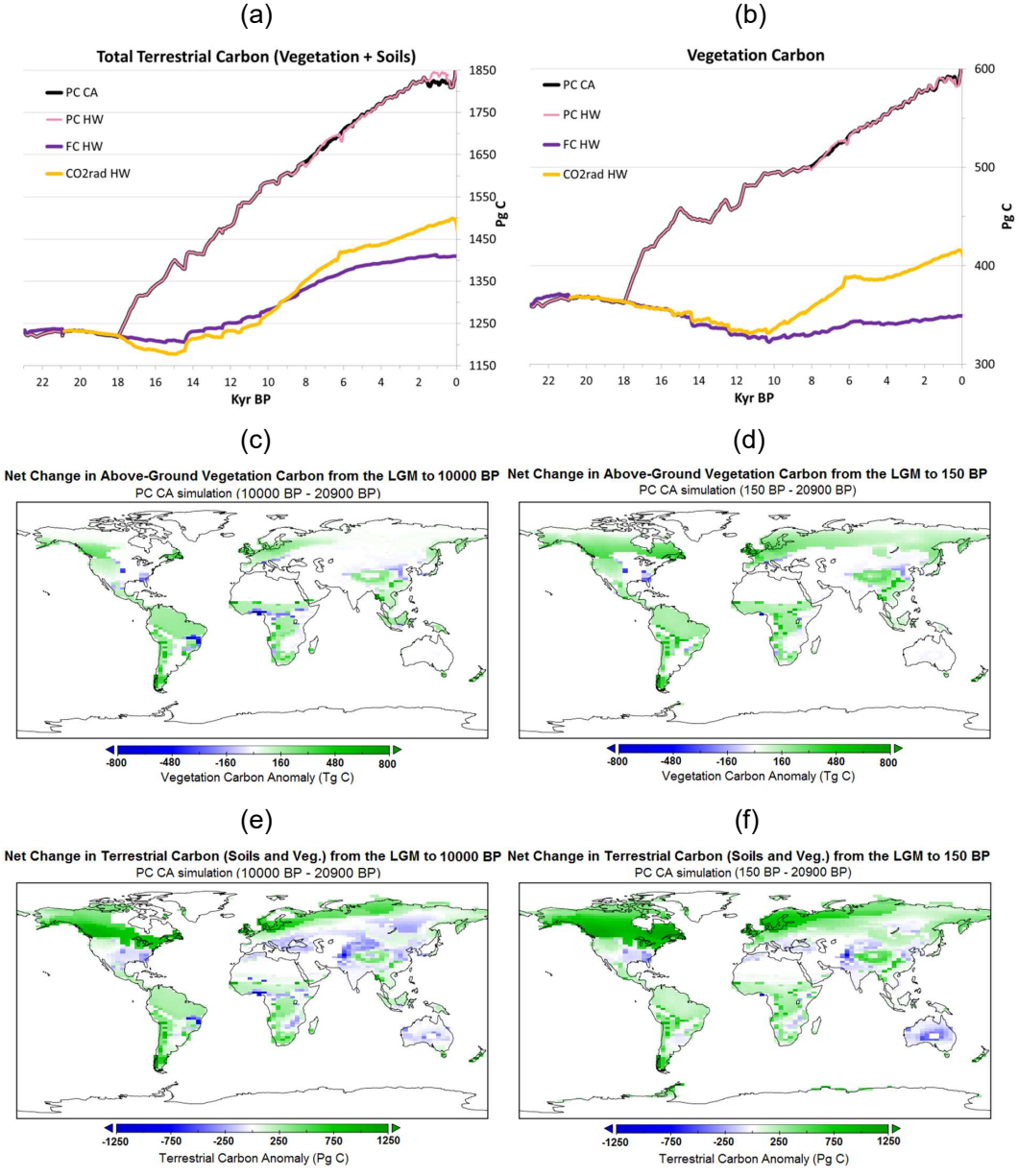


*Fig. 3: Time series of (a) global terrestrial carbon (vegetation and soils) and (b) above-ground vegetation carbon for a Prescribed Carbon simulation with constant alkalinity (PC CA, black line) and Prescribed Carbon with the higher (12 Tmol yr$^{-1}$) weathering rate (PC HW, pink line). The FC HW and CO2rad HW results (from Fig. 1) are plotted for comparison. In (c-f), vegetation carbon and total terrestrial carbon changes from the LGM are mapped as in 2(a-d) for the PC CA simulation.*

Clim. Past Discuss., doi:10.5194/cp-2016-24, 2016
Manuscript under review for journal Clim. Past
Published: 17 March 2016


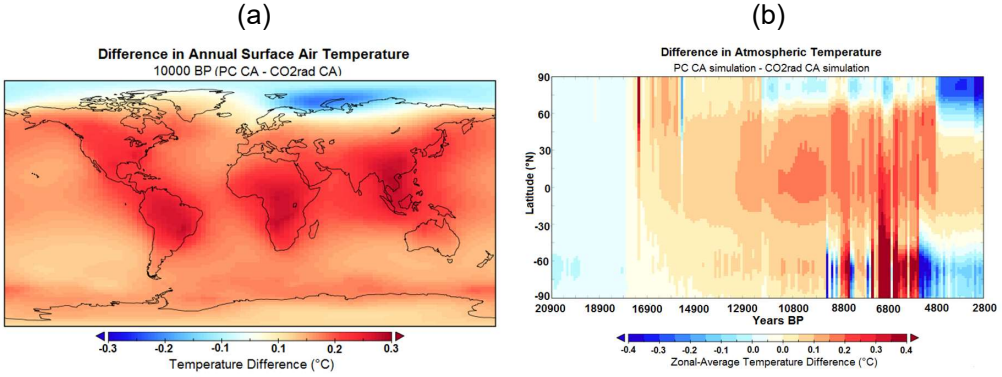


*Fig. 4 : Surface air temperature differences between the PC CA simulation and the CO2rad CA simulation, both of which have equivalent $CO_2$ radiative forcing. In (a), a time slice is provided for 10000 BP, which corresponds to the terrestrial and vegetation carbon stocks shown in Fig. 3 for the PC CA simulation). In (b), a Hovmöller diagram shows the zonal-average surface air temperature difference between the two simulations with time.*

Clim. Past Discuss., doi:10.5194/cp-2016-24, 2016
Manuscript under review for journal Clim. Past
Published: 17 March 2016


Climate of the Past Discussions
Open Access
EGU

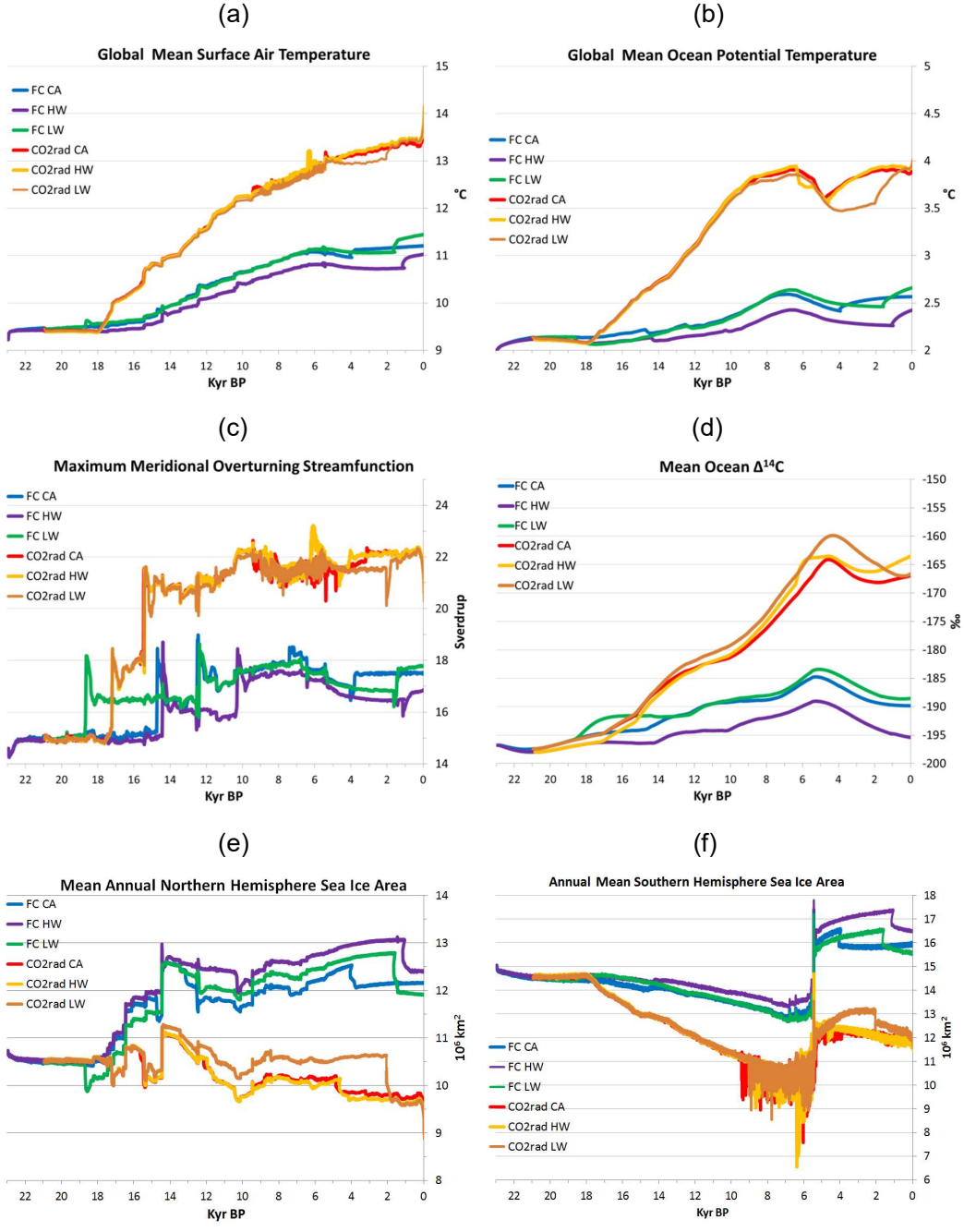


*Fig. 5: Time series of (a) global mean surface air temperature (9°C to 15°C ), (b) volume-weighted mean ocean potential temperature (2°C to 5°C), (c) global maximum ocean meridional overturning streamfunction value (14 Sv to 25 Sv), (d) volume-weighted mean ocean $\Delta^{14}C$ (-200‰ to -150‰) under a constant atmospheric $\Delta^{14}C$ of 0‰ for all simulations, (e) mean annual Northern Hemisphere sea ice area (8 -14×10⁶ km²), and (f) mean annual Southern Hemisphere sea ice area (6-18×10⁶ km²). The colours representing each simulation are as in Fig. 1.*

Clim. Past Discuss., doi:10.5194/cp-2016-24, 2016
Manuscript under review for journal Clim. Past
Published: 17 March 2016


Climate of the Past
Discussions
Open Access
EGU

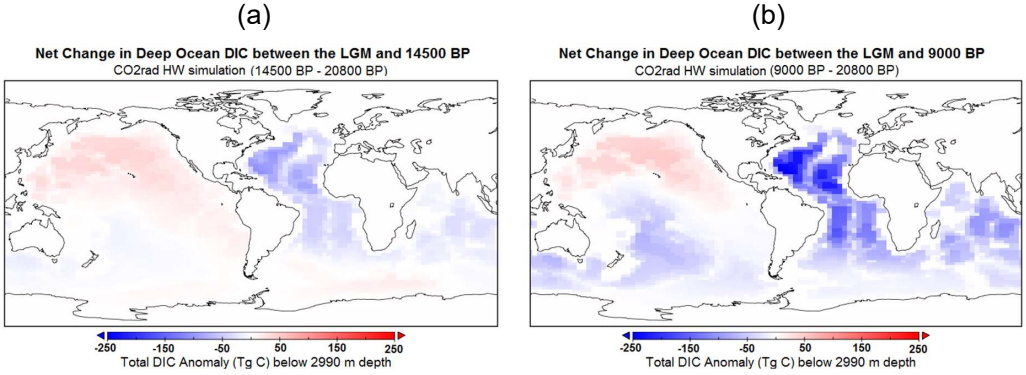


*Fig. 6: The net change in deep-ocean DIC (below 2990, the deepest 31.2% of the model ocean) in Tg C between the LGM and (a) 14500 BP and (b) 9000 BP in the CO2rad HW simulation, both on a scale from -250 Tg C (blue) to +250 Tg C (red).*

Clim. Past Discuss., doi:10.5194/cp-2016-24, 2016
Manuscript under review for journal Clim. Past
Published: 17 March 2016


Climate of the Past Discussions
Open Access
EGU

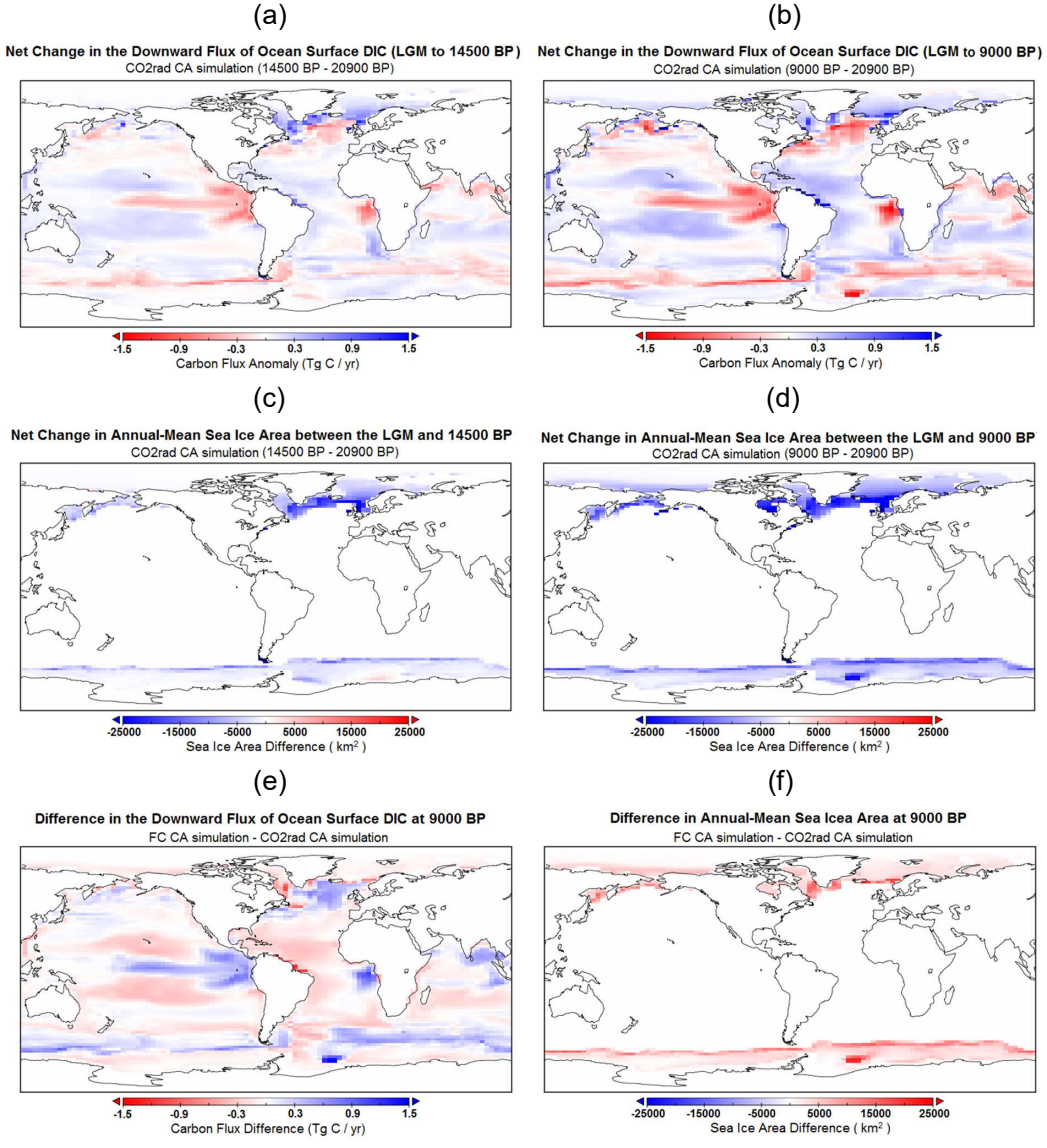


*Fig. 7: The spatial distribution of the net change in the downward flux of inorganic carbon at the ocean surface between the LGM (-1.5 to +1.5 Tg C $yr^{-1}$) and (a) 14500 BP and (b) 9000 BP. Regions with greater outgassing (or less downwelling) than the LGM are shaded in red, whereas areas with greater uptake (or more downwelling) are blue. These are compared to the net change in annual-mean sea ice area since the LGM (-25000 to +25000 $km^2$) at (c) 14500 BP and (d) 9000 BP, with area losses relative to the LGM shaded in blue and gains shaded in red. In (e-f), the differences in (e) surface inorganic carbon flux and (f) sea ice area between the FC CA and CO2rad CA simulation at 9000 BP are given. Blue (red) shading represents less (more) outgassing in the FC CA simulation relative to the CO2rad CA simulation in (e) and red indicating greater sea ice area in the FC CA simulation relative to the CO2rad CA simulation at 9000 BP in (f).*

Clim. Past Discuss., doi:10.5194/cp-2016-24, 2016
Manuscript under review for journal Clim. Past
Published: 17 March 2016


Climate of the Past Discussions
Open Access
EGU

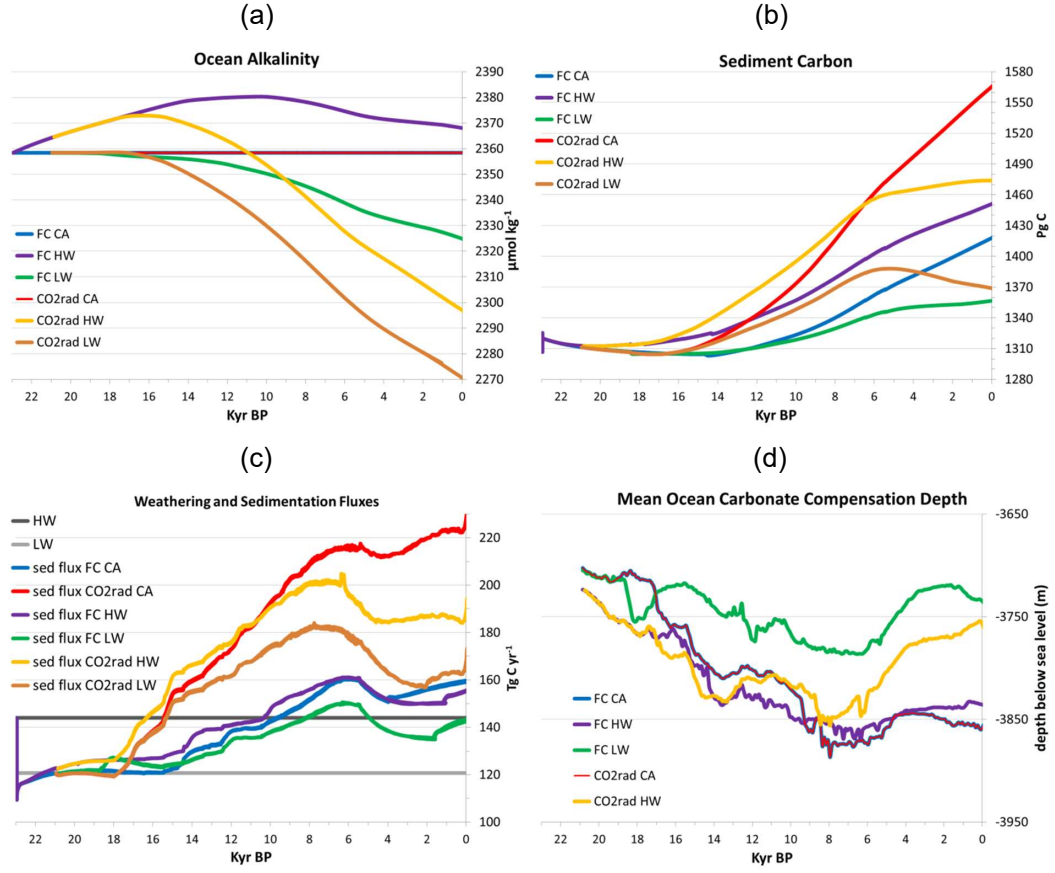


*Fig. 8: As in Fig. 1, for variables related changes in ocean alkalinity. In (a), changes in total mean ocean alkalinity ( $[HCO_3^-] + 2[HCO_3^{2-}]$ ) are given in µmol $kg^{-1}$ (with a plot range from 2290 to 2390 µmol $kg^{-1}$). In (b), the total change in sediment carbon (Pg C) are provided on a different scale (1280 to 1580 Pg C) than in Supplementary Fig. 1d. In (c), weathering fluxes (constant HW and LW rates are represented by a dark grey and light grey line respectively) and sedimentation fluxes (coloured lines) are provided. For the CO2rad CA and FC CA simulations, only the sedimentation rate is plotted, as by definition the weathering rate and sedimentation rates are exactly equal in these simulations. In (d), the carbonate compensation depth (CCD), calculated as the depth where sedimentation flux is equal to the dissolution flux (above which 99-100% of sedimentation occurs in the model) is provided with a scale range from 3950m to 3650 m depth.*

Clim. Past Discuss., doi:10.5194/cp-2016-24, 2016
Manuscript under review for journal Clim. Past
Published: 17 March 2016


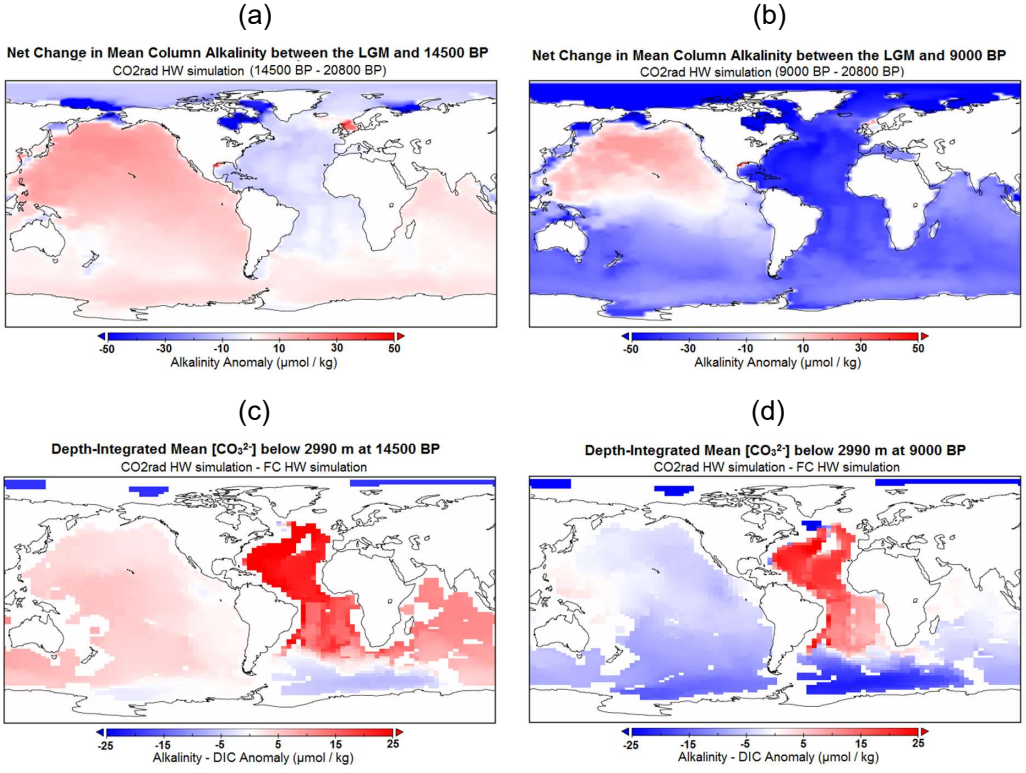


*Fig. 9: The spatial distribution of alkalinity anomalies (a-b) since the LGM in the CO2rad HW simulation, and Alkalinity-DIC (~[$CO_3^{2-}$]) differences (c-d) between the CO2rad HW and FC HW simulations. In (a-b), the net change in the the total column mean alkalinity (average depth-integrated alkalinity for each gridcell) between the LGM and (a) 14500 BP and (b) 9000 BP is given. In (c-d), the column (depth-integrated mean) Alkalinity-DIC below 2900 m depth in the CO2rad HW simulation is subtracted from that of the FC HW simulation at (c) 14500 BP and (d) 9000 BP*

Clim. Past Discuss., doi:10.5194/cp-2016-24, 2016
Manuscript under review for journal Clim. Past
Published: 17 March 2016


Climate of the Past Discussions
Open Access
EGU

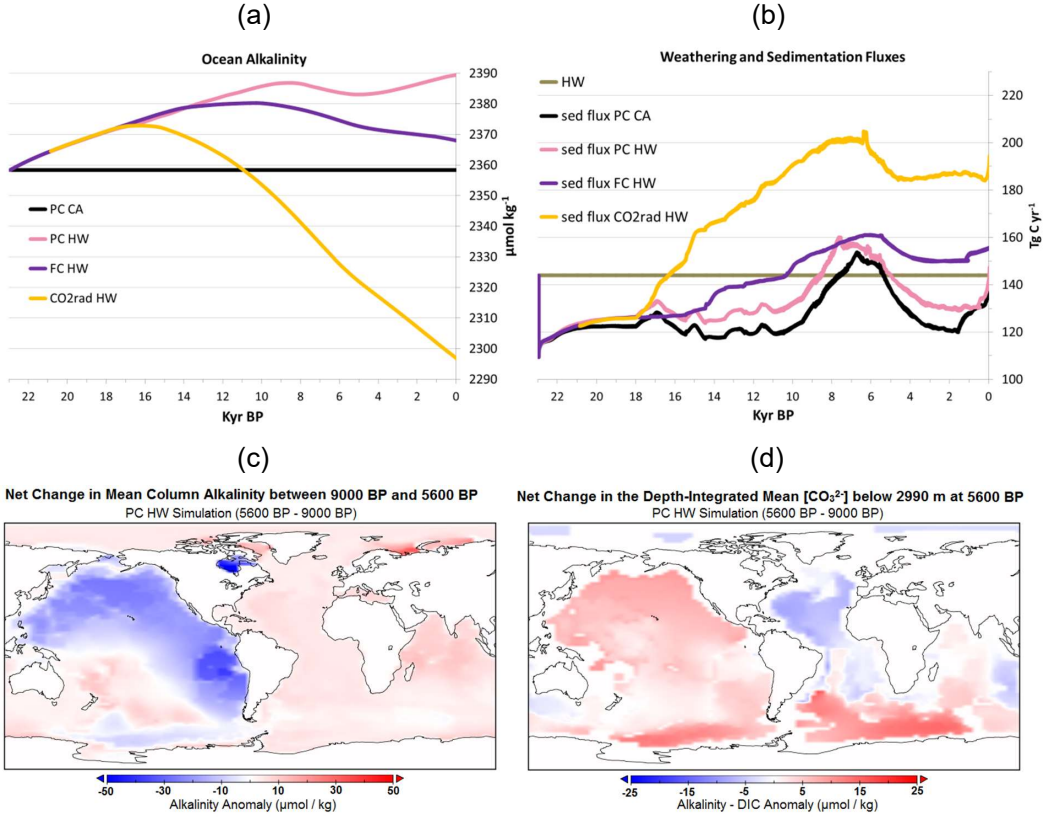


*Fig. 10: The time series for (a) ocean mean alkalinity and (b) weathering and sedimentation fluxes are given, as in Fig. 8a,c. Only the sedimentation flux is plotted for PC CA in (b) because, by definition, weathering rates and sedimentation rates are equivalent in this simulation. For the PC HW simulation, in (c) the mean total column depth-integrated alkalinity change between 9000 BP and 5600 BP is given at each gridcell, whereas in (d) the net change in mean column depth-integrated[Alk-DIC] below 2990 m depth is provided for the same time interval.*

Clim. Past Discuss., doi:10.5194/cp-2016-24, 2016
Manuscript under review for journal Clim. Past
Published: 17 March 2016


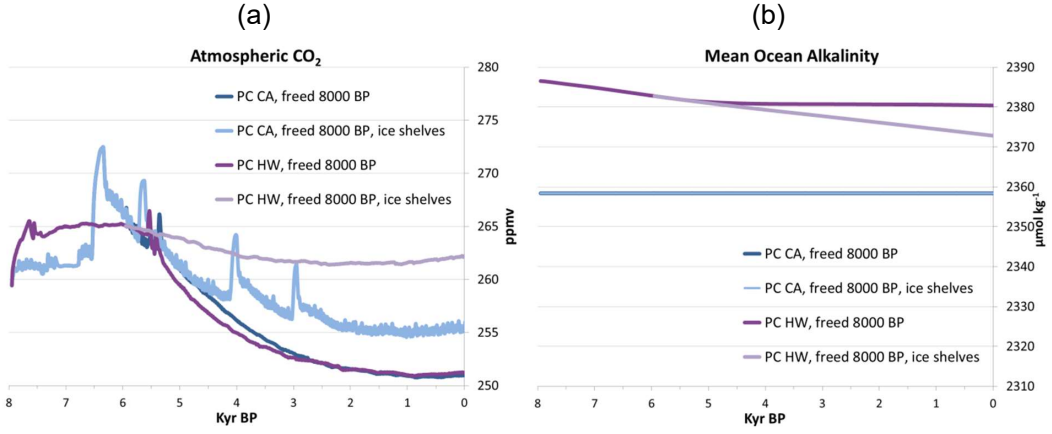


*Fig. 11: The PC CA and PC HW simulations repeated with a freed carbon cycle after 8000 BP, including different Antarctic marine ice shelf configurations. In the legend, "freed 8000 BP." indicates that no further carbon was injected into the atmosphere (after 8000 BP), whereas "ice shelves" indicates a simulation where marine ice shelves in the interpolated ICE-4G dataset were held fixed after 6000 BP, as in Simmons et al. (2013). Trends in (a) atmospheric $CO_2$ and (b) ocean alkalinity are portrayed for these simulations. Note that the time scale for both figures is different than in the other time series in this paper.*

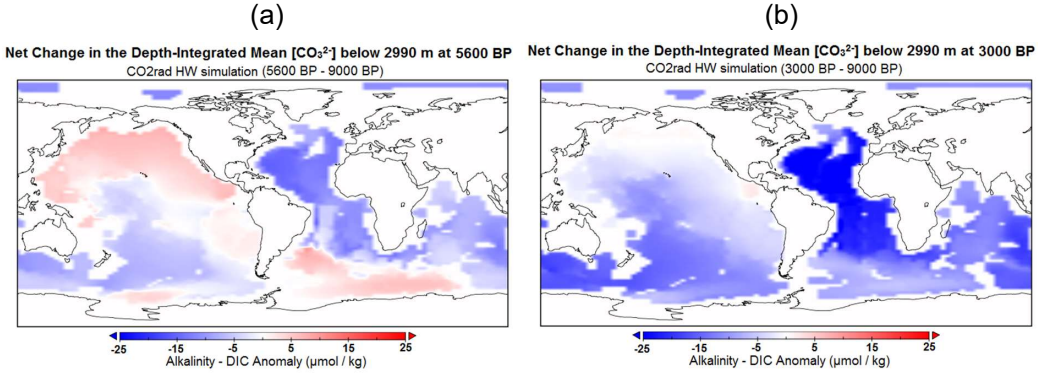


*Fig. 12: The net change between 9000 BP and (a) 5600 BP and (b) 3000 BP in the depth-integrated column (gridcell) average Alk-DIC below 2990 m depth.*